

BRNO UNIVERSITY OF TECHNOLOGY

VYSOKÉ UČENÍ TECHNICKÉ V BRNĚ

CENTRAL EUROPEAN INSTITUTE OF TECHNOLOGY BUT

STŘEDOEVROPSKÝ TECHNOLOGICKÝ INSTITUT VUT

SMART NANODEVICES

CHYTRÉ NANONÁSTROJE

NANOSCALED POLYPYRROLE FOR SENSING GASEOUS ANALYTES AND VOLATILE ORGANIC COMPOUNDS

NANO-POLYPYRROL PRO DETEKCI PLYNNÝCH ANALYTŮ A TEKAVÝCH ORGANICKÝCH LÁTEK

DOCTORAL THESIS

DIZERTAČNÍ PRÁCE

AUTHOR

AUTOR PRÁCE

Milena Šetka, M.Sc.

SUPERVISOR

ŠKOLITEL

doc. Ing. Jana Drbohlavová, Ph.D.

CO-SUPERVISOR

ŠKOLITEL SPECIALISTA

Dr. Stella Vallejos Vargas

Abstract

Polypyrrole (PPy) is a hetero-cyclic conductive polymer (CPs) with chemical structure based on the existence of conjugated electrons between alternating single and double bond system. This polymer has occupied the attention of many scientists from different research disciplines due to its outstanding properties such as good electrical conductivity, relatively high environmental stability, and facile and diversified synthesis methods. The aim of this research was to study the sensing behavior of PPy. Therefore, the gas sensing performances of PPy nanostructures were verified to ‘gas molecules of high importance’ including acetone, ammonia, ethanol, ethylene and toluene.

In this work, PPy in the form of nanorods (NRs) and nanoparticles (NPs) was prepared using electrochemical and chemical synthesis approaches, respectively. Additionally, the modified PPy structures were developed by functionalization of PPy NPs with catalytic particles of gold (Au), silver (Ag) and cadmium-telluride (CdTe). Many complementary analytical techniques (microscopic and spectroscopic) were used for the investigation of morphology, composition and structure of the synthesized materials. Moreover, spectroscopy techniques such as Raman and X-Ray Photoelectron Spectroscopy (XPS) were employed for *in-situ* gas sensing tests, which confirmed the potential of PPy NRs and PPy NPs to be used as gas sensitive materials.

In order to developed the gas sensor device, the PPy based materials were integrated into chemo-resistive and Love mode surface acoustic wave (L-SAW) transducing platforms. The gas sensing test of chemo-resistive sensors based on PPy NRs revealed negligible response to nitrogen dioxide and ammonia due to complicate architecture of those sensors. The measuring of response of non-modified and modified PPy NPs chemo-resistive sensors was complex due to their extremely high resistance in $G\Omega$ range. However, multi-guiding L-SAW sensors based on bare PPy NPs and modified with Au NPs and Ag NPs, and CdTe quantum dots (QDs) manifested the response to low concentration of all tested target gas molecules including ammonia, acetone, ethanol, ethylene and toluene at room temperature (RT). Generally, the L-SAW sensors with modified sensing layers established enhanced sensing performances over non-modified sensors. The performance of the L-SAW sensor primarily depends on the operating frequency and the choose of sensitive layer in the active region of the sensor. Thus, among the tested sensing layers for the target gases, modified PPy layer with Ag NPs and/or Au NPs can be selected as the best option for the detection of acetone.

The developed PPy based L-SAW sensors are simple and cost effective devices with improved sensing properties such as high sensitivity and low limit of detection (LOD) which make them potential candidates in future systems for air quality control, food quality control or disease diagnosis via exhaled breath.

Key words

Polypyrrole, surface acoustic wave, gas sensors, volatile organic compounds.

Abstrakt

Polypyrol (PPy) je heterocyklický vodivý polymer s chemickou strukturou založenou na existenci systému konjugovaných elektronů mezi střídajícími se jednoduchými a dvojnými vazbami. Díky svým vynikajícím vlastnostem jako je dobrá elektrická vodivost, relativně vysoká stabilita prostředí a zároveň i jednoduchost a variabilita metod jeho přípravy, přilákal tento polymer pozornost mnoha vědců z různých vědních disciplín. Cílem výzkumu v této dizertační práci byla studie senzoričného chování PPy. Za tímto účelem byla ověřena účinnost nanostruktur PPy při detekci vybraných „vysoce důležitých molekul plynů“ včetně acetonu, amoniaku, etanolu, etylenu a toluenu.

V této práci byl připraven PPy ve formě nanotyčinek (NRs) pomocí elektrochemické syntézy a také ve formě nanočástic (NPs) chemickou cestou. Dále byly připraveny modifikované PPy struktury, a to funkcionalizací PPy NPs katalytickými částicemi zlata (Au), stříbra (Ag) a teluridu kademnatého (CdTe). Pro charakterizaci morfologie, složení a struktury připravených materiálů bylo použito několik komplementárních analytických (mikroskopických i spektroskopických) technik. Navíc byly využity techniky jako Ramanova a rentgenová fotoelektronová spektroskopie (XPS) pro in-situ test detekce plynů, které potvrdily potenciál připraveného materiálu, tedy PPy NRs i PPy NPs, pro využití v senzorech plynů.

Za účelem výroby senzoru plynů byl připravený PPy materiál integrován do dvou typů převodníkových platforem: chemorezistivní a na bázi povrchové akustické vlny v tzv. Love módu (L-SAW). Test detekce plynů pro chemorezistivní senzory s PPy NRs ukázal pouze zanedbatelnou odpověď těchto senzorů pro oxid dusičitý a amoniak z důvodu jejich komplikované architektury. Změření odzvy tvou typů chemorezistivních senzorů-nemodifikovaného i modifikovaného PPy NPs nebylo možné z důvodu extrémně vysoké odporu v řádu GΩ. Nicméně multivodivé L-SAW senzory založené na holých PPy NPs či PPy NPs modifikovaných Au či Ag NPs a nebo CdTe kvantovými tečkami (QDs) vykazovaly odezvu pro nízké koncentrace všech testovaných velmi důležitých molekul plynů při pokojové teplotě (RT). Obecně měly L-SAW senzory s modifikovanou citlivou vrstvou vyšší citlivost než senzory s nemodifikovanou PPy citlivou vrstvou. Účinnost L-SAW senzoru primárně závisí na pracovní frekvenci a na výběru citlivé vrstvy v aktivní oblasti senzoru. Z otestovaných typů vrstev senzoru vůči jednotlivým plynům, modifikovaná PPy NPs s Ag NPs i Au NPs se javí jako nejlepší varianta pro detekci acetonu.

Připravené L-SAW senzory na bázi PPy jsou jednoduchá a cenově přijatelná zařízení s vylepšenými detekčními vlastnostmi jako je vysoká senzitivita a nízký limit detekce (LOD), což je řadí mezi potenciální kandidáty v budoucích systémech pro kontrolu kvality vzduchu, potravin a rovněž pro diagnostiku nemocí z dechu.

Klíčová slova

Polypyrol, povrchová akustická vlna, plynové senzory, volatilní organický látky.

Bibliographic citation

Milena Šetka. Nanoscaled polypyrrole for sensing gaseous analytes and volatile organic compounds. Doctoral Thesis. Brno University of Technology, Central European Institute of Technology. Brno, 2020. Supervisor Jana Drbohlavová.

Contents

Abstract	i
1 Introduction	1
1.1 Motivation	1
1.2 Aims of the thesis	2
2 Literature review	3
2.1 Classification of sensing materials	3
2.1.1 Metal oxides	4
2.1.2 Conductive polymers	4
2.2 Polypyrrole gas sensors	7
2.3 Introduction to gas sensors	8
2.3.1 Transducing principles	9
2.4 Gases and VOCs of high importance	10
2.4.1 Acetone	10
2.4.2 Ammonia	11
2.4.3 Ethanol	11
2.4.4 Ethylene	11
2.4.5 Toluene	12
3 Polypyrrole nanorods and nanoparticles	13
3.1 Experimental	13
3.1.1 Synthesis of PPy NRs	13
3.1.2 Synthesis of PPy NPs	13
3.1.3 Material analysis and <i>in-situ</i> gas sensing test	14
3.1.4 Fabrication of PPy NRs based chemo-resistive sensors	15
3.2 Results	15
3.2.1 Physical and chemical characteristics of the PPy NRs and PPy NPs.	15
3.2.2 <i>In-situ</i> gas sensing test	17
3.2.3 Ammonia and nitrogen dioxide test of PPy NRs based chemo-resistive sensors	19
3.3 Conclusions	20
4 Love wave sensors based on polypyrrole modified with catalytic metal nanoparticles	21
4.1 Experimental	21
4.1.1 Synthesis of Au/PPy	21
4.1.2 Synthesis of Ag/PPy	21
4.1.3 Fabrication of L-SAW sensor	22
4.1.4 L-SAW sensors characterization	22
4.1.5 Gas sensing tests	22
4.2 Results	23
4.2.1 PPy and Au/PPy L-SAW sensors	23
4.2.2 PPy and Ag/PPy L-SAW sensors	25
4.3 PPy NPs chemo-resistive sensors	27
4.4 Conclusions	27

5	Love wave sensor based on polypyrrole modified with CdTe quantum dots	28
5.1	Experimental	28
5.1.1	Synthesis of CdTe QDs	28
5.1.2	L-SAW sensor fabrication	28
5.1.3	Characterization of sensing materials	28
5.1.4	Gas sensing test	29
5.2	Results	29
5.2.1	Characterization of the sensitive materials	29
5.2.2	Gas sensing test	30
5.3	Conclusions	32
6	Summary of results and conclusions	33

Chapter 1

Introduction

1.1 Motivation

The development and investigation of gas sensors become the subject of great importance because of their potential implementation in various areas such as environment monitoring, food quality, and health diagnosis [1, 2, 3]. Many efforts have been devoted in developing of gas sensing materials with high sensing capabilities to target analytes. Nanomaterials have undoubtedly gained the most of the attention among scientists as gas sensors functional layers, due to their high surface to volume ratios and unique chemical or physical gas adsorption capabilities resulting in enhanced sensitivity [4]. Moreover, nanoscale morphology gives possibility for easy surface modifications of the active layer of gas sensor using a relatively simple and cost effective fabrication methods [2].

Among different materials, inorganic materials, such as metal [2] and metal oxides (MOX) [5, 6] represent the most widespread sensing layers for gas sensors. Mostly, from the group of MOX, semiconductor oxides (e.g., WO_3 , ZnO , SnO_2 , In_2O_3 , etc.) have been extensively investigated [7]. In addition, the doping of host sensing material with nanostructures of noble metals have been reported to increase its chemical activity and enhance the sensing properties of gas sensors. Among the metallic elements employed for gas sensors are palladium (Pd) [8], platinum (Pt) [9], Au [10], Ag [11], etc. Another category used for gas sensors are carbon based materials, thanks to their high quality crystal lattices and high carrier mobility (e.g. ballistic charge transport) [12]. The most frequently studied carbon nanomaterials in gas sensors application are namely carbon nanofibres, carbon nanotubes, graphene and reduced graphene oxide [13].

From organic materials, CPs represent an important class for next generation of chemical gas sensors [14, 15]. CPs either individually or in a hybrid form, i.e., in the combination with other materials such as various noble metals (e.g., Ag [16, 17], Au [18], Pd [19]), MOX (e.g., ZnO [20], SnO_2 [21]), carbon-based materials (e.g., carbon nanotubes [22, 23] or various forms of graphene [24, 25]) were used for the development of the sensing layers. CPs such as PPy [26, 27], polyaniline (PANI) [28, 29], polyacetylene (PA) [30, 31], polythiophene (PTh) [32], and poly(3,4 ethylenedioxythiophene) (PEDOT) [33, 34] are considered as most promising materials for gas sensing applications. Among hetero-cyclic CPs, PPy captured the wide attention of the scientific community due to its facile and diversified synthesis methods, its good electrical conductivity and relatively high environmental stability. Therefore, it has been used not only in gas sensing but also in electrodes for batteries [35], supercapacitors [36] and biosensing [37].

Metal and MOX gas sensors require very high operating temperatures (from 200 °C [38, 39] up to 400 °C [40, 41], or even higher [42]) which turn into high power consumption. This is a primary issue, especially for the autonomy of portable battery-powered devices. To overcome this problem, it is necessary to accomplish sensitive layers from novel materials, which allow sensing of the gaseous analytes at RT. In particular, the main advantage of the above mentioned CPs is their capability of working at RT, which make them outstanding candidates compared to most MOX. The creation of composite materials by functionalization of CPs with e.g., catalytic metals or MOX showed better gas sensing performances compared with the single component, especially higher response, lower LOD and faster response [43].

The monitoring of the gases and volatile organic compounds (VOCs) in exhaled breath has gained a considerable scientific, clinical, and research attention due to its potential in enabling the non-invasive observation of the biochemical processes of the human body. Specific gases and VOCs can be considered as relevant biomarkers related to different diseases especially variety of pulmonary diseases (chronic

obstructive pulmonary disease, lung cancer, asthma, cystic fibrosis, respiratory tract infection), and other diseases such as colorectal cancer, breast cancer, and they could aid the early diagnosis of those diseases [44, 45, 46, 47, 48, 49].

Apart from the breath analysis, specific gases and VOCs are classified as air pollutants and they are considered as essential parameters for assessing the air quality in indoor and outdoor environments (e.g., emission from industrial processes, traffic activity, waste treatment and disposal, tobacco smoking, etc.) [50]. Moreover, detection of different gases and VOCs is used for food quality analysis in order to determine the freshness and spoilage of food [51].

The detection of analytes such as ammonia, acetone, ethanol, ethylene and toluene in very small amounts, in the sub-ppm range, is of great significance for assessment of potential environmental pollution, human health risks, diseases diagnosis and food spoilage. Nowadays, the detection of those target gases in the breath analysis, food and/or air quality requires large and expensive laboratory equipment such as gas-chromatographers, ion-mobility spectrometers and mass spectrometers [51, 52, 53, 54, 55]. Recently, the gas sensors also have found a new potential in such applications, where development of novel sensing materials and their utilization for the detection of the gaseous markers have attracted wide attention among many researchers. This attractive research direction could have a huge social impact with the possibility of the costs reduction, and affecting, in turn, the quality of life.

Therefore, my dissertation topic was focused on developing of a micro scalable gas sensor to enable monitoring of low concentration levels of the target analytes defined above which are relevant in air and food quality control or disease diagnosis. Keeping in mind the main advantage of CPs (working at RT), the sensing properties of PPy and its combinations with other decorative/functional materials were examined, discussed, and compared in this work.

1.2 Aims of the thesis

The main aim of this thesis is to develop sensor devices based on a unique combination and integration of nanostructured PPy sensing materials and transducing techniques. The performance of this device was verified by monitoring low concentrations of specific gases and VOCs including acetone, ammonia, ethanol, ethylene and toluene, which are classified as relevant markers involved in breath analysis, food quality analysis and/or environment monitoring.

To achieve this goal, the thesis is divided into the following specific objectives:

1. Synthesis of nanoscaled functional films (e.g., NRs, NPs) based on PPy via chemical and/or electrochemical methods.
2. Study of composition and structure of the synthesized PPy materials as well as investigation of their chemical activity and potential to be used as sensing material.
3. Surface modification of the nanoscaled PPy with different catalytic metals (e.g., Au, Ag) or QDs (e.g., cadmium based core/shell structures) followed by determination of chemical composition of those inorganic-organic composites.
4. Gas sensing tests of both non-modified and surface modified PPy films to target gases and VOCs through measurements of variation in electrical conductivity or changes in surface acoustic wave (SAW) characteristics due to analyte sorption.

Chapter 2

Literature review

2.1 Classification of sensing materials

The gas sensing materials are a key component which play a critical role in the performance of gas sensors. According to their nature, all gas sensors can be classified into three groups: MOX [56], CPs [14] and carbon based materials [13, 57], as it is shown in Figure 2.1. In general, the main requirements of gas sensing material are the ability to show a high sensitivity and selectivity in contact with target species. Additionally, the sensing layer is supposed to interact reversibly and reproducibly with the specific analyte of interest, and show a strong stability in a harsh environment conditions such as high temperature and/or high relative humidity (RH). From the economical point of view, the molecular recognition layer should be widely available, simply and inexpensively synthesized, compatible and easily implemented with a specific transducing platforms.

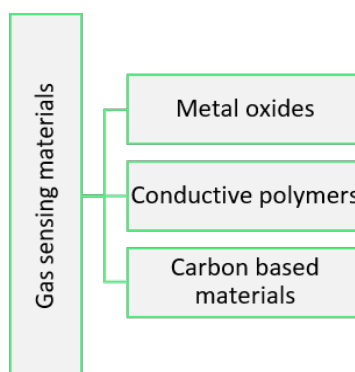


Figure 2.1: Classification of gas sensitive materials.

All mentioned types of gas sensing materials showed the markedly different sensing characteristics with the competing advantages over each other due to different nature of analyte adsorption process and sensing mechanism between specific material and target analyte [4]. The summary of advantages and limits of gas recognition materials is presented in Table 2.1. Generally, the particular drawbacks for single sensing materials, namely, high operating temperature and low selectivity for MOX, poor chemical stability and deficient selectivity for CPs, and poor reproducibility, long term stability and high cost of carbon based materials, can restrict their practical application.

In order to conquer the above mentioned specific issues, several possibilities have been suggested as an alternative strategies for enhancement of gas sensing performances by many researchers [43, 58, 59, 60]:

- the functionalization and doping of host recognition materials with other components,
- creation of hetero-junctions (interface between two dissimilar semiconductor materials with different band gap),
- and utilization of inorganic/organic hybrid materials.

Table 2.1: Summary of Gas Sensitive Materials. The data is adapted from [61].

Type of material	Advantages	Limiting factors
MOX	Small size Low cost Short response time Long-lasting life Simple circuit	Poor specificity and selectivity High operating temperature Affected by humidity and poisoning Non-linearity at high temperature High energy consumption
CPs	Strong sensitivity Room operating temperature Strong biomolecular interactions Various preparation processes	Long response and recovery time Low selectivity Easy affected by humidity
Carbon based materials	High sensitivity Strong adsorption capacity Stable and suitable for mixing with other materials Quick adsorption capacity	High cost Complicated production Non-uniform standard Complex mechanism

Additionally, the gas sensing properties can be enhanced by morphological and dimensional control, specifically by structuring materials to 0 dimensional (D) (e.g., NPs and QDs), 1D (e.g., nanofibers, nanotubes, NRs, and nanowires), 2D (e.g., thin films, nanosheets and nanoplates) and 3D (e.g., hierarchical structures assembled from NPs, NRs, nanosheets, etc.). These forms with the high surface area may provide more active sites for the sorption of gas [60].

2.1.1 Metal oxides

Semiconductor MOX nanostructures and thin films have been widely adopted for detection of different gases and VOCs. Those structures are mostly implemented into chemo-resistive transducing platforms [62], but also they found application in the field of SAW [63] or optical sensors [64]. There are two main types of semiconducting MOX based sensors, n-type (whose majority carrier are electrons) and p-type (whose majority carrier are holes). Both, n-type (e.g., ZnO, WO₃, etc.) and p-type (e.g., CuO, NiO, etc.) oxides were tailored to various shapes (e.g., NRs, nanowire, nanotubes etc.) with different aspect ratio (μm -nm scale) and used as the recognition layer for gas sensors [65]. In general, the MOX gas sensors showed enhanced sensing properties with high sensitivity towards many analytes including specific gases and VOCs (selected in Section 2.4) [66]. However, the main drawback of those sensors which restricts their development is a high operational temperature (even up to 500 °C). Thus, high cost and complicated configuration of those sensors is noticed in comparison to others system working at RT.

The formation of hetero-junctions by coupling of two different n-types and/or n and p-type of MOX have been reported in the literature as a new strategy for improvement of gas sensing performance [60, 68]. Therefore, the gas sensing studies of the composite MOX structure, namely cerium oxide-tungsten oxide core-shell nanowires (n-n hetero-junctions) were also explored in this thesis. The results are summarized in the article [67], (*Cerium oxide-tungsten oxide core-shell nanowire-based microsensors sensitive to acetone*). Indeed, the structures with hetero-junctions demonstrated an increased response and sensitivity in comparison to non-modified tungsten oxide wires or cerium oxide porous films based sensors. The gas sensing test of those sensors to specific gases and VOCs (ethanol, acetone, toluene, carbon monoxide and hydrogen) was carried out at the temperature range between 150-400 °C. Those studies confirmed the above mentioned requirements (in terms of high operation temperature) of MOX based sensors and shifted the focus of this thesis to exploration of properties of CPs in gas sensing.

2.1.2 Conductive polymers

Polymers are organic materials and most of them belongs to the category of insulators since they are made by covalent bonds without free movable charge carriers (electrons or ions). However, CPs are a specific category of synthetic polymers which opened a new era in science and technology due to their

distinctive electrical and optical properties which are similar to those of semiconductor MOX or even metals. CPs, namely PA, were discovered by Heeger, MacDiarmid and Shirakawai in 1977 and authors were awarded the Nobel Prize in Chemistry in 2000 [69]. The structure of PA is shown in Figure 2.2. CPs found extensive application in the field of rechargeable batteries, electrochromic display devices, polymeric light emitting diodes, photovoltaic devices, biosensor and gas sensor [14, 70, 71, 72].

The conductivity of CPs originates from highly delocalized electrons between the conjugated polymer backbone (alternating single bonds (σ) and double bonds (π)) and the dopant (negatively charged species). The delocalized π -electrons freely move along the entire chain of polymer and the dopant removes an electron from a delocalized bonding arrangement, creating a hole. Afterwards, an electron from neighbouring molecule jumps and fits that hole generating a new hole and allowing charge to flow through the polymer chain [69]. Therefore, the choice of dopant and doping level determine the conductivity of CPs [74].

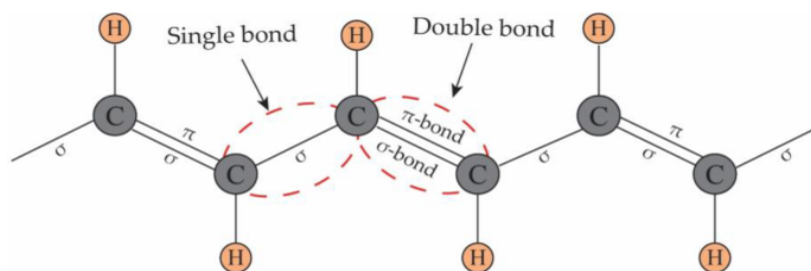


Figure 2.2: The structure of PA: the backbone contains conjugated double bonds, where π bonds move along the carbon chain. The image is adopted from [73].

The charge carriers of CPs are called a polarons and bipolarons. A polaron is defined as a radical ion (spin $\frac{1}{2}$) associated with a lattice distortion and localized electronic levels within the band gap after removal of an electron. A bipolaron is defined as a pair of like charges (dication) associated with a strong local lattice distortion after removal of second electron where the decrease in the energy gap occurred [73, 75].

Most of nanostructured CPs with different morphology (e.g., 0D, 1D, or 3D) have been synthesized by oxidative polymerization between corresponding monomer and an oxidizing agent using chemical or electrochemical techniques [76]. A different synthesis conditions and approaches induce the differences in the morphology and structure of CPs, which are unquestionably a crucial factors affecting their physical and chemical properties. Various synthesis strategies have been used for CPs fabrication, which can be categorized under two main approaches: template based synthesis (hard templates) and template free approaches (soft templates) [71, 77, 78, 79].

1. The template based synthesis used a physical template to guide grow of nanostructures in designed shapes and sizes. The most common hard templates are nano sized channels such as anodic aluminum oxide (AAO) and particle track-etched membranes (e.g., polycarbonate or polyester) [80, 81]. Those type of synthesis routes are effective for controlling of homogeneity, length, and diameter of nanostructures, while their main disadvantage is a post-synthesis removal of the template.
2. The soft template approaches are a relatively simple and cheap fabrication process where polymerization of CPs is based on self assembly of various types of surfactants micelles [81, 82, 83]. Those methods do not require a template or potentially harsh post-synthesis treatment.

The CPs have been used as the sensitive layers of gas sensors since early 1980s. They have been in the spotlight of research investigations particularly thanks to their conductivity and operation at RT, but also due to easy synthesis, chemical and structural diversity, and flexibility. CPs such as PPy, PANI, PTh, and PEDOT, and their derivatives have been the most studied candidates for sensing layers [84, 85, 86]. The interaction between those CPs and chemical species of interest can cause a change in electrical, piezoelectric or optical properties of the active layer. Therefore, the CPs have found application in chemo-resistive [87, 88], mass [89, 90] and optical gas sensors [91, 92]. The structure of typical CPs used in gas sensing is presented in Figure 2.3.

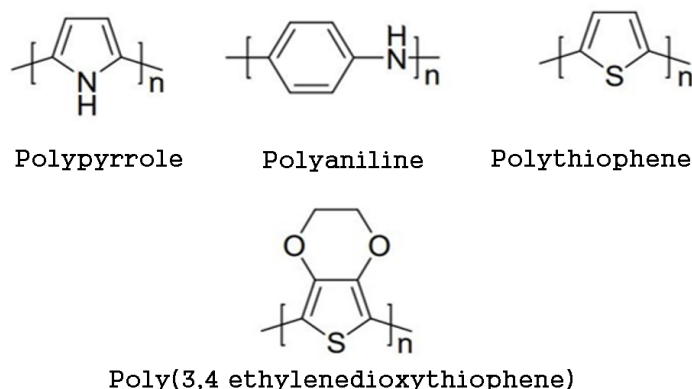


Figure 2.3: Chemical structure of polypyrrole (PPy), polyaniline (PANI), polythiophene (Pth) and Poly (3,4 ethylenedioxythiophene) (PEDOT).

The most widely used gas sensors based on PPy, PANI, PTh and PEDOT are chemo-resistors and their sensing performances to different gases (e.g., ammonia, nitrogen dioxide, carbon dioxide, etc.) and VOCs (e.g., methanol, ethanol, acetone, etc.) were intensively investigated [14, 93, 94, 95]. Ammonia have been very often studied as the target species of those sensors and the responses to this analyte are compared and presented in Table 2.2.

Table 2.2: Summary of sensing properties of various CP chemo-resistive based sensors to ammonia. Response of sensor is defined as $R = R_g/R_a$, where R is response of sensors, and R_a and R_g are resistance in air and gas, respectively. The response of sensor (R) is defined for the tested concentration (C).

Type of CPs	Modification	Morphology	R	C (ppm)	Ref.
PPy	-	Film	1.1	20	[97]
	-	Thin film	1.5	50	[98]
	SnO ₂	Nanofiber	2.8	2.5	[87]
	Reduced graphene oxide	Film	1.1	1	[99]
PANI	-	Film	1.6	50	[100]
	-	Nanofibrous	2.4	10	[101]
	SnO ₂	Porous sphere	5.4	10	[88]
	Quasi-graphite capsules	3D hollow	1.1	5	[102]
PTh	-	Film	1	100	[103]
	Reduced graphene oxide	Fiber	2.2	10	[104]
PEDOT	-	Film	1	500	[105]
	Graphene	Film	1	50	
	-	Nanotube	1.0	20	[107]
	Ag	Film	1.3	15	[108]

In general, all tested sensing CP materials showed the positive response to ammonia. However, the ratio of response magnitude to concentration value of PPy and PANI based sensors is slightly higher compared to other mentioned polymers. These observations were reported in the review paper about “*Conducting Polymers as Chemiresistive Gas Sensing Materials*” [84]. The enhanced responses of PPy and PANI may be partially assigned to their particular morphology, but also to the doped states (especially their nature and concentration) which affect the degree of oxidation and control the electrical conductivity in polymers [96]. The sensors based on hybrids of PPy, PANI, PTh and/or PEDOT with another material (e.g. MOX, noble metals or carbon based materials such as graphene) showed increased sensing properties over bare materials. As mentioned above, this can be related to the creation of functionalized material which possesses a new or improved electronic, magnetic, and optical properties in comparison with non-modified CPs.

2.2 Polypyrrole gas sensors

According to our literature survey based on state of the art PPy gas sensors, which is presented in a journal article [106], nanostructures with different shapes such as NPs, NRs, nanowires, nanotubes, nanoplates, nanoribbons, etc., were used as the gas sensing materials. These nanostructures were developed using both, electrochemical than chemical synthesis approach based on either template or template-free methods.

Table 2.3: Overview of PPy used as active layers for detection of ammonia and VOCs at room temperature.

Morphology	Analyte	LOD (ppm)	Transducing Mechanism	Ref.
PPy nanoparticles	Ammonia	5	Chemo-resistive	[110]
Multidimensional PPy nanotubes	Ammonia	0.01	Chemo-resistive	[111]
Single PPy nanowire	Ammonia	40	Chemo-resistive	[85]
PPy nanowires	Ammonia	1.5	Chemo-resistive	[15]
Single crystal PPy nanotube	Ammonia	0.00005	Chemo-resistive	[112]
PPy nanoribbons	Ammonia	0.5	Chemo-resistive	[114]
PPy/ZnO nanocomposite	Ammonia	10	Chemo-resistive	[21]
PPy/SnO ₂ nanocomposite	Ammonia	10	Chemo-resistive	[21]
Au/PPy nanopeapods	Ammonia	0.007	Chemo-resistive	[113]
PPy nanoparticles	Methanol Acetonitrile Acetic acid	50 100 100	Chemo-resistive	[110]
Multidimensional PPy nanotubes	Ethanol	1	Chemo-resistive	[111]
Nanotubular PPy	Butanol Propanol Methanol Ethanol	3 for all alcohols	Chemo-resistive	[115]
Au/PPy nanorods	Benzene Toluene Acetic acid	10 for all analytes	Optical	[116]
PPy fibres	Methanol Ethanol Acetone Toluene Chloroform Isopropyl alcohol	1 for methanol 10–30 for other VOCs	Optical	[117]
Al/PPy/Au/dodecylbenzene sulfonic acid diodes	Methanol	20 ppm	Capacitive	[118]
PPy films	Acetone	10 ppm	Capacitive	[119]
Single PPy nanowire	Heptanal Acetophenone Isopropyl myristate 2-Propanol	9 0.8 134 130	Chemo-resistive	[120]
PPy film	Acetone Ethanol Isopropyl alcohol	-	Impedance	[121]
PPy film	Methanol Acetone Ethyl acetate Ethanol	-	Impedance	[122]

Generally, both synthesis methods refer to the oxidative polymerization of the monomer pyrrole. While electropolymerized PPy is achieved using an appropriate electrolyte solution (pyrrole and an oxidizing agent) under constant applied voltage or current in an electrochemical cell, chemically polymerized PPy is achieved via wet chemical synthesis by the oxidation of pyrrole with an oxidizing agent such as FeCl_3 , LiClO_4 . The final properties of PPy in both synthesis methods are strongly dependent on factors such as concentration, type of oxidizing substance and solvent. Apart from those factors, the electropolymerization of PPy also depends on the applied voltage and current density. The electrochemical synthesis enables a wide choice of oxidizing agents, and localized control over material thickness and geometry, whereas the chemical synthesis provides the ability to generate nanostructures in a continuous, rather than batch mode. The latter implies higher throughput and simpler instrumentation.

The literature review showed that PPy gas sensors working on a chemo-resistive transducing principle have received much more attention among the scientists than the other ones (e.g., optical, SAW, capacitance, impedance). The most frequently these sensors were tested for the detection of ammonia and some VOCs (e.g. alcohols, ketones, aromatic hydrocarbons), see Table 2.3. Overall, it is difficult to note significant differences in the sensing properties of the described sensors, however, they have been strongly dependent on the morphology of sensitive layer. For instance, the lowest LOD of 0.05 ppb was found for single crystal PPy nanotube sensors for ammonia, while sensors based on multidimensional PPy nanotubes showed the lowest LOD of 1 ppm to ethanol. Generally, the enhanced sensing properties (e.g., sensitivity) of the PPy sensors have been noticed for the structures with smaller size due to their higher active surface area. Beside PPy size and morphology, its functionalization with various nanosized materials like noble metals, metal oxides and different types of carbon was found to have a crucial effect on the final sensitivity and usually resulted in enhanced sensor performance.

In conclusion, the presented works demonstrated that either in single or modified form, PPy can be successfully used for gas sensing. Despite their great advantages such as RT operation, high sensitivity and short response time, some functional issues such as poor selectivity and modified sensor response in humid atmosphere have been found challenging [123, 106]. The development of nanocomposite material with favourable properties and chemical versatility may help to overcome those limitations, and hence, promote an effective detection of specific gases and VOCs [94, 124]. Thus, the interest in future investigation and development of hybrid materials with the desired properties is expected in the field of gas sensors.

In this context, the work in this thesis was focused on the studies of non-modified and modified PPy nanostructures and their integration into sensing devices for the detection of target gases and VOCs.

2.3 Introduction to gas sensors

A chemical gas sensor can be described as a device that transforms chemical information into an analytically useful signal (e.g., electrical, optical), which can be measured and quantified directly or indirectly. The receptor (i.e., gas sensitive material) and transducer are two main parts of chemical sensors. The transformation of chemical information into a form of energy is responsibility of the receptor, while the transducer converts that energy into analytical signal [125].

The main functional characteristics of gas sensors include sensitivity, selectivity, response time, recovery time, and reversibility [126]. Depending on the type of transducing mechanism, these parameters may vary a lot and have a significant influence on the final feature of the sensor. The meaning of each parameter is specified below:

- **Sensitivity** of sensor measures a magnitude of output signal which is produced as the response to an input quantity of given magnitude. Generally, the response of gas sensors is expected for the tested analyte concentration in range of ppm or even ppb.
- **Selectivity** can be defined as the ability of sensor to respond primarily to only one species in the presence of other analytes. However, complete selectivity of gas sensor is usually desired but very often hard to achieve.
- **Response time** is defined as the necessary time to reach 90 % of the total value of measured electrical change.
- **Recovery time** is defined as the time required for measured signal to return to 90 % of the original value, when sensor exposure is switched from the target gas to carrier gas (synthetic air or some halogen gas). Both, response and recovery times should be as fast as in units of seconds.

- **Reversibility** is the ability of a sensor to recover, or return to its original background/baseline condition, after exposure to an analyte.

Apart of the mentioned sensors characteristic and their desired magnitudes, there is also a need for production of simple, inexpensive and low-power devices in order to fulfill the economical requirements.

2.3.1 Transducing principles

The gas sensors can be classified according to the method for monitoring of gas-solid interactions (type of transducing mechanism), and they can be divided into two main groups:

- **electrochemical** (conductometric, amperometric and potentiometric)
- **electromechanical** (optical, gravimetric and calorimetric) sensors.

In this thesis, chemo-resistive (type of conductometric) and SAW (type of gravimetric) sensors are investigated. The operating principle of chemo-resistive gas sensors is based on the change in their electrical conductivity caused by a reaction between gaseous chemical species and receptor (sensing material). The reaction between gas and sensitive layer is believed to occur by the adsorption of oxygen in the surface, leading to an increase or decrease of electrical resistance of the sensitive layer after the exposure to an oxidative or reductive target gas, respectively (considering an n-type semiconductor) [127]. Typically, these sensors are designed from two parts:

1. electrodes (mostly interdigital) which are patterned on an insulating substrate (silicon, alumina),
2. and a conductive sensing layer (e.g. MOX, CPs and/or carbon based materials) which is embedded to electrodes.

The sensors are usually connected to direct current (DC) bridge configuration. During the measurements, DC voltage is applied to the electrodes and the electrons are traveling in the sensitive layer between two electrodes. When the target gaseous analyte is adsorbed at the sensitive layer, the change in electrical resistance occurs and this change is monitored as a sensor response.

SAW sensors rely on disturbance and changes in the mass of sensitive layer during the interaction with analysed gases. The mass vibrations (changes) on the mechanical resonator (piezoelectric substrate) are caused by the absorption of a gas on sensitive layer which induce a shift in the operating frequency of resonator. The resonator motion (displacement, rotation, strain) is converted into the electrical signal which is measured as the sensor response [128]. SAW gas sensors are mostly based on **Rayleigh** and **Love waves**. Rayleigh waves propagate along a free surface or on the boundary between two materials with the particle motion in longitudinal and transverse directions which follows a retrograde elliptical path. The most of wave energy is localized in the near surface region of an isotropic solid and the amplitude of wave is decreasing with depth [130]. Love waves exist in the surface layer when the shear wave velocity of the upper layer is less than that of the lower layer. The waves are trapped in the upper layer and the particle motion is parallel to free surface and perpendicular to the direction of propagation [130]. The Love waves are guided close to the sensing surface by confining the wave energy in thin guiding layer. The guiding layer slows the velocity of wave with respect to the piezoelectric substrate and make the surface highly sensitive to small perturbation.

The SAW gas sensors are composed of:

- piezoelectric substrate,
- IDTs,
- wave guiding layer (in the case of Love wave),
- and sensitive layer.

The structure of the SAW sensor with the guiding and sensitive layer on the top of piezoelectric substrate is presented in Figure 2.4.

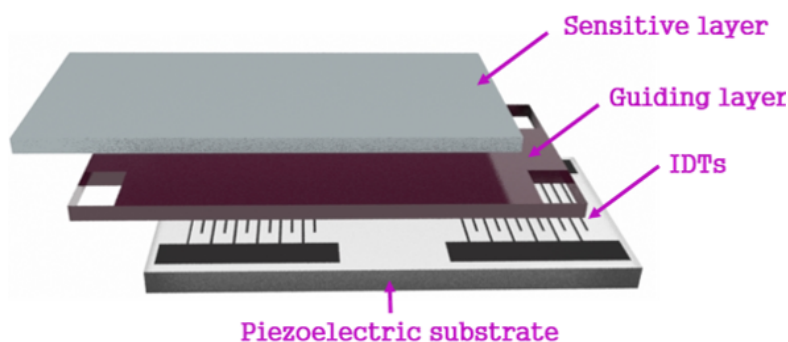


Figure 2.4: The structure of L-SAW sensor contains of piezoelectric structure, IDTs, guiding and sensitive layer. When the wave is guided through both, guiding and sensitive layer, that structure is known as multi-guiding.

The important characteristics of SAW gas sensor, such as sensitivity, selectivity, LOD, repeatability, and stability depend critically on the physical and chemical properties of sensing layer, device design, operation frequency and environmental conditions such as temperature and RH. In principle, SAW gas sensors offer ultra-high sensitivity, fast response, suitable size and structure, and ability to work in wireless mode [132, 133]. Therefore, PPy based L-SAW sensors were chosen and investigated as the suitable candidates in this thesis.

2.4 Gases and VOCs of high importance

The profile of gases and VOCs which are classified as markers for different applications (e.g., breath analysis, air or food quality monitoring) is wide and complex. In order to design a sensor for multiple applications, it is necessary that the selected gases and VOCs of interest are overlapping. Thus, some gases and VOCs including acetone, ammonia, ethanol, ethylene and toluene) are classified as the target gases in this thesis, as their detection has a great impact in various applications.

2.4.1 Acetone

Acetone (C_3H_6O) has a sweetish taste with a characteristic odour of decaying apple and it has been found in different concentration levels in the exhaled breath of almost every person. During the history, acetone has been known as a breath biomarker for diabetes mellitus, however, only acetone cannot be used to diagnose and monitor diabetes. The increased acetone levels in the range of 0.22 to 9.41 ppm [135] have been found in the breath of diabetic patients [135, 136], but also in the breath of lung cancer patients (112–2654 ppb) in comparison with healthy people (42–753 ppb) [137]. The reported acetone concentrations can vary from disease to disease and from patient to patient and it can be affected by several factors such as age, food consuming (fasting), medicines, addiction behaviour, lifestyle, and/or profession [138]. For instance, overnight fasting and/or a ketogenic diet (low carbohydrate diet) can raise the levels of acetone in the exhaled breath in healthy individuals [139]. Thus, there is a need for additional studies and combination of acetone with other breath biomarkers which may help to indicate glycaemia [135, 138, 139].

The increased concentration of acetone vapours has been also reported in indoor air. It can originate from different solvents such as furniture polish, cleaning products (e.g., bleach, laundry detergent, etc.), nail polish remover, floor glue, and oil paint [140, 141]. Breathing of acetone in moderate to high amounts for a short time can cause an irritation of nose, throat, lungs and eyes. It can also cause headaches, dizziness, confusion, a faster pulse, nausea, vomiting, effects on the blood, passing out and possible coma, and a shorter menstrual cycle [142]. American Conference of Governmental Industrial Hygienists (ACGIH) sets the occupational threshold limit values (TLV) for acetone to 250 ppm, considering 8-h time-weighted averages.

Also, acetone is one of ketone that is present as an aroma compound in many foods and used as the quality marker. For instance, it was identified as a good marker to characterize the freshness of various type of fish (e.g., tuna, salmon, cod) due to its accumulation during fish spoilage [51]. Moreover, acetone was identified in contaminated apples and used as marker of high bacterial content [143].

2.4.2 Ammonia

Ammonia (NH_3) is classified as a toxic air pollutant with an unpleasant odour that can harm the human body, namely causing the damage to the respiratory tract, eyes, and skin, inflammation or inhibition of the cell growth [144]. The presence of ammonia in atmosphere originates from different sources like chemical or automotive industry, agricultural sector, farming, etc. [145]. The concentration of this gas in natural atmosphere is very low (sub-ppb levels), while for instance its concentration can reach more than 10 ppm near intensive farming areas. The concentration of 50 ppm is tabulated as lower limit of human ammonia perception by smell, nevertheless, ammonia may cause irritation to respiratory system, skin and eyes even at lower concentration [146]. TLV value for ammonia is set to be 25 ppm (based on 8-hour time weighted average) by ACGIH.

In human body, ammonia is processed in the liver, kidneys and skeletal muscles. The ammonia path through a body of healthy individuals is followed by its conversion into urea in the liver and urea is then transported through the bloodstream and excreted into urine by the kidneys. The excessive level of ammonia in blood is noted in the patient with kidney dysfunction due to an impaired removal of waste products (e.g., urea) from the blood. The surplus ammonia molecules as well as other nitrogen-containing volatile compounds can diffuse into the lungs and be found in higher concentrations (92–4240 ppb) in the breath of patients with chronic kidney disease in comparison to healthy controls (43.2–830 ppb), and serve as the relevant biomarker of renal disease [147, 148].

Total volatile basic nitrogen (TVB–N) content is an important indicator for evaluation of meat freshness. Ammonia is one of the main component of TVB–N, its levels increase with a spoilage by either bacterial or enzymatic degradation and it can be used as a marker of meat freshness [149, 150].

2.4.3 Ethanol

Ethanol ($\text{C}_2\text{H}_6\text{O}$) is a volatile alcohol which is extensively used in a broad range of industries such as biomedical, chemical, food, pharmaceutical, etc. The accurate detection of ethanol is very important and necessary in various applications, including the quality of alcoholic beverages (e.g. wine, beer) [151], quality control of food [152], indoor air quality [141], breath analysis (e.g. breath alcohol test of drivers, clinical diagnosis) [137, 153].

Ethanol is an important marker used for monitoring of fermentation processes during the alcoholic beverages production and determination of characteristics of final products (e.g., aroma, flavour, quality, etc.) [151, 154]. Additionally, ethanol is also used for the estimation of food spoilage, namely, it was used as effective index for freshness characterization of peach [155]; the increased concentration of ethanol was found in the various types of fish (e.g., whiting, mackerel, cod) after storage for 10 days and used to determine the spoilage stages of fish [134].

Ethanol is presented in a relatively low concentration around 200 ppb in human breath of healthy individuals. Its level in the breath is significantly increased after alcohol consumption, thus, ethanol is used as the marker of drunkenness level of drivers [156]. Also, the increased concentration of ethanol has been found in the breath of lung cancer patients (13–1520 ppb) in comparison with healthy subjects (4–480 ppb) [137]. Before the ethanol values in exhaled breath are linked to specific pathological processes and this volatile is used as a biomarker, it is necessary to take into account other sources of ethanol in breath. Hence, the increased ethanol concentration may be affected by its production by mouth flora or gut microflora after consumption of sugars [156], and/or by its contribution in the inhaled ambient air [157].

Considering effect of the inhaled vapours of ethanol on human health, the concentration of ethanol (observed in industrial fields with fermentation and distillation) can cause irritation of the skin, inflammation of the nasal mucous membrane and conjunctiva, while at high levels, it can cause even alcohol poisoning [153]. 1000 ppm is the maximum permitted concentration of ethanol vapour in the work place (defined by ACGIH).

2.4.4 Ethylene

Ethylene (C_2H_4) is a gaseous plant hormone which plays a crucial role in many phases of plant biology, such as growth, development, pathogen infection, fruit ripening, storage of fruit [158, 159]. It is generated in the plants during their maturity. In the agricultural and food industry, ethylene concentration in range of ppb-ppm levels has been used as a maturity index to determine the time of harvest. During post-harvest in storage room and transportation chains, the control of ethylene concentration is necessary, as the specific concentration of this gas can be either beneficial or deleterious for different types of

fruits. For instance, climacteric fruits (e.g., banana, kiwi, avocado) are usually artificially ripened by ethylene in order to extend their shelf-life and ensure shelf-maturity; however, the excess concentration of ethylene can increase its auto-catalytic production in the fruit and cause accelerated maturation, senescence and even spoilage [160]. The sensitivity between ethylene concentration and fruit ripening varies in the storage conditions, namely, 10 ppm of ethylene is used to induce ripening of bananas [161], while continues exposure to 10 ppb of ethylene can affect mandarin quality [162].

Ethylene contained in the human breath is considered as a biomarker of oxidative stress. The production of ethylene in the body is connected with the oxidative degradation (lipid peroxidation) of polyunsaturated fatty acids caused by reactive oxygen species. Ethylene is highly volatile gas which is not significantly metabolized by the body and not soluble in body fat, thus its diffusion into bloodstream after generation is rapid. After its transportation to the lungs, it is excreted in the expired breath. Thus, ethylene in the exhaled breath can be considered as a novel biomarker of the infection and oxidative stress with potentially important clinical implications [163, 164, 165]. The low concentration of ethylene is found in the breath of healthy humans (around 6.3 ppb), while its concentration is increased in the breath of patient with renal failure (around 150 ppb) [147, 166].

From an environmental point of view, ethylene is considered a precursor pollutant being involved in the creation of ozone at ground level, which is seriously harmful for human health [167]. Ethylene in the atmosphere originates mostly from natural sources (emissions from vegetation) and anthropogenic sources (emission from incomplete engine combustion, industry, cigarette smoke, natural gas leaks) [168]. The ACGIH lists ethylene as a simple asphyxiate gas.

2.4.5 Toluene

Toluene (C_7H_8) is an aromatic hydrocarbon, classified as a chronic toxicant which causes eye, nose, and throat irritation, drowsiness and dizziness in low concentrations (below 100 ppm), while a neurological damage and dysfunction of the central nervous system (e.g. moderate performances of short-term memory, attention and concentration, visual scanning, perceptual motor speeds, colour vision and auditory capacity) is a principal health outcome of exposure to high concentration of toluene [169, 170, 171]. For instance, the concentration of toluene exceeding 200 ppm can cause a fatigue, headache, paresthesias, and slowed reflexes, while confusion develops at levels of 600 ppm or above, and euphoria appears as levels near 800 ppm [171]. The principal sources of toluene in the environment originate from evaporation and combustion of various industrial products (e.g., petrol, paint, adhesives, coating, tobacco smoke, etc.). ACGIH limits the TLV of toluene to 20 ppm. In the human breath, toluene is considered among the VOCs with exogenous origin and it has been reported very often as a marker of smoking habits. The average concentration in the breath of smokers (9–153 ppb) is significantly higher compared to non-smoker breath [156, 172, 173].

Chapter 3

Polypyrrole nanorods and nanoparticles

The outputs associated to specific objective 1 and 2 of this thesis are summarized in this section. The synthesis of PPy NPs and PPy NRs was achieved via chemical and electrochemical approaches and complemented with their morphological, compositional studies and *in-situ* sensing test to ammonia. These results are published in a journal article, *Raman and XPS studies of ammonia sensitive polypyrrole nanorods and nanoparticles* [174]. The results related to the sensing test of PPy NRs based chemo-resistive sensors are also included here and published in a conference article, *Gold/polypyrrole nanorods for gas sensing application* [175].

3.1 Experimental

3.1.1 Synthesis of PPy NRs

PPy NRs were synthesized on the top of Au NRs via template-based electrochemical polymerization enabled by a two-electrode system under potentiostatic (constant potential) mode. Silicon wafers with thermally oxidized silicon dioxide layer (1.5×1.5mm) covered, from bottom to top, by sputter-deposited titanium (Ti, 20 nm thick), tungsten (W, 150 nm thick) and aluminium (Al, 500 nm thick) were used as a substrate (Figure 3.1 a). The deposition of above mentioned layers was performed using RFICP Kaufman ion-beam source, KRI®. In the first step, the electrochemical anodization of Al and W was performed under 40 V in 0.3 M oxalic acid at 10 °C. These conditions led to the formation of nanoporous AAO template (Figure 3.1 b) with tungsten trioxide (WO₃) nanodots (Figure 3.1 c) at the bottom which were subsequently etched in a phosphate buffer solution (pH=7, T=25 °C). This step allowed the formation of W nanodimpled surface (Figure 3.1 d) as a base for the growth of the Au NRs (Figure 3.1 e). The pulsed galvanic deposition of Au was carried out in potassium dicyanoaurate solution under following conditions: 35 pulses, pulse length of 400 ms, a period of 2 s between pulses, a current of 1 mA, and a potential of 5 V. Then PPy was deposited under a voltage of 2 V for 120 s during the electrochemical polymerization (Figure 3.1 f). The PPy was formed in a mixture of pyrrole monomer and anionic doping salt, tetraethylammonium tetrafluoroborate, with the molar ratio of 2:1, dissolved in acetonitrile solvent. These synthesis conditions resulted in creation of Au/PPy NRs in form of a 'sandwich structure' (Figure 3.1 g), where NRs are connected from the bottom part with the metallic layer of W (100 nm thick) and from the top part covered with the over deposited layer of PPy (100 nm thick). To clean the surface and eliminate any over deposition of the PPy, the polymer layer was etched using oxygen plasma with applied power of 100 W at 50 mTorr and a gas flow of 50 sccm of O₂ for 15 min. Finally, the AAO template was selectively dissolved in the aqueous solution of chromium trioxide and phosphoric acid at 60 °C for 600 s.

3.1.2 Synthesis of PPy NPs

PPy NPs were obtained via oxidative chemical polymerization of pyrrole monomer based on the formation of complex between water-soluble polymer polyvinyl alcohol (PVA) and FeCl₃ in aqueous solution, as described previously [110]. Briefly, 7.5 g of PVA was diluted in 92.5 ml of distilled water and stirred till all PVA was completely dissolved. Subsequently, 3.73 g of FeCl₃ was added to the solution; after this step, a change of color from transparent to yellow was observed. The stirring was continued for 5 min until an equilibrium was established, then 0.69 cm⁻³ of pyrrole monomer was dropped in the reaction mixture.

As soon as the pyrrole mixed with the oxidant (FeCl_3), a rapid polymerization reaction occurred. This turned the solution into a characteristic black color that indicates the formation of PPy. The stirring process was kept constant for 5 h. Finally, PPy NPs were drop-coated on silicon tiles ($1.5 \times 1.5 \text{ mm}$) and dried at 80°C for 30 min.

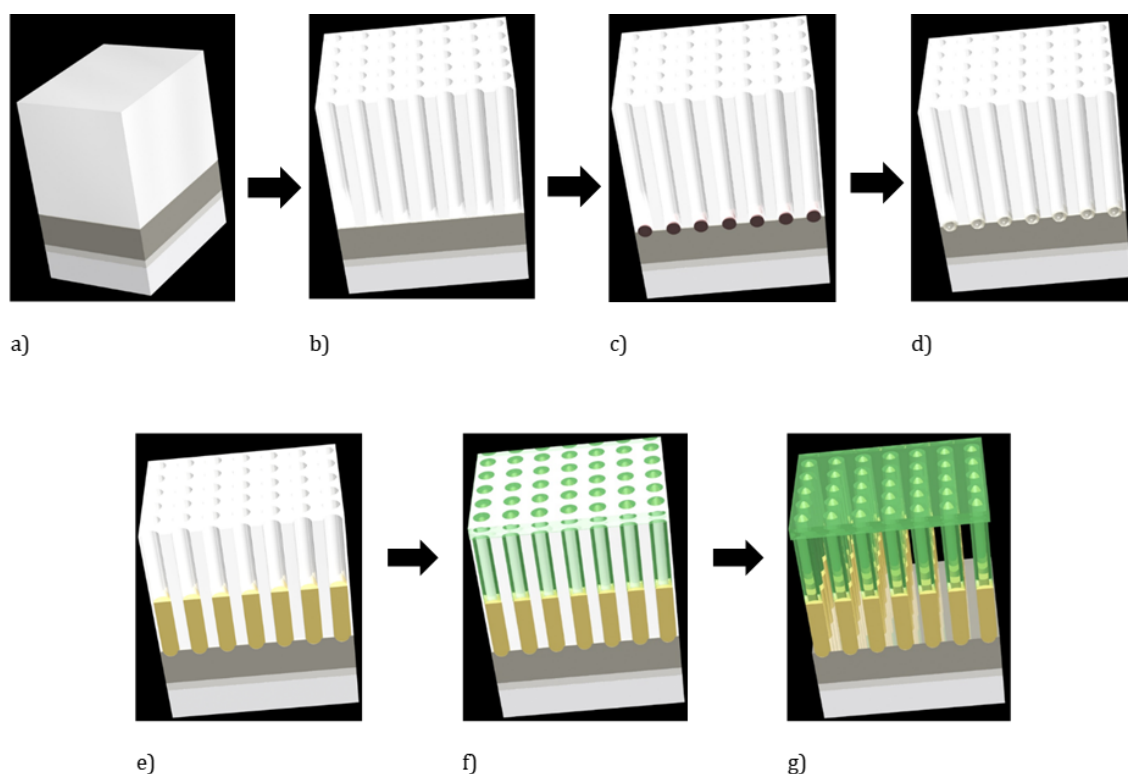


Figure 3.1: Schematic illustration of the fabrication process of PPy NRs; From bottom to top Si wafer covered with: $1 \mu\text{m}$ SiO_2 , 20 nm Ti , 150 nm W , and 500 nm Al (a); AAO template after the electrochemical anodization of the Al in 0.3 M oxalic acid (b); AAO template after the oxidation of W , and creation of WO_3 nanodots (c); AAO template after the etching of WO_3 nanodots in phosphate buffer forming the nanodimpled surface (d); Au deposition using potassium dicyanoaurate solution (e); PPy deposition using solution of pyrrole monomer and TEABF_4 in acetonitrile (f); Au/PPy NRs in form of ‘sandwich structure’ after the selective etching of AAO template (g).

3.1.3 Material analysis and *in-situ* gas sensing test

Scanning Electron Microscopy (SEM) and Transmission Electron Microscopy (TEM)) were used for the morphological analysis of PPy NRs and PPy NPs. The structural characterization and *in-situ* gas sensing test of PPy NRs and PPy NPs was performed using Raman and XPS analysis. Raman analysis was carried out using a Renishaw InVia Raman microscope employing 785 nm and 633 nm laser beam for PPy NRs and PPy NPs, respectively. The spectra were recorded using a power lower than 1 mW and a $20\times$ objective. Raman spectra were recorded at 60°C . During the measurements, the samples were placed in a chamber equipped with a continuous gas flow system. Nitrogen was used as reference and simultaneously as a carrier gas for the saturated ammonia vapour which was produced by bubbling ammonia (Panreac, $30\% \text{ w/v}$) at RT. Thus, PPy NRs and PPy NPs samples were exposed either to nitrogen or 0.3% of ammonia for 5 min . Afterwards, the Raman spectra were recorded. After ammonia exposure, the samples were cleaned in nitrogen flow for 15 min . The Raman spectra before and after ammonia exposure presented in this work were recorded on the same sample and site. Moreover, the same procedure was repeated in various sites of the sample to confirm the tendency of the spectra.

In order to further study the mechanisms of ammonia detection, the PPy NRs and PPy NPs were exposed to ammonia flow for 20 min at 60°C and subsequently, the XPS spectra were recorded. These analyses were performed on the same samples used for Raman. The XPS spectra before and after ammonia were measured in various nearby sites. XPS was carried out using Kratos AXIS Supra

spectrometer with monochromatic $K\alpha$ X-ray radiation, emission current of 15 mA, hybrid lens mode and charge compensation on. High-resolution spectra were collected with analyser pass energy of 20 eV and with 0.1 eV energy resolution. The deconvolution of all XPS data was elaborated using Casa XPS v.2.3.18 software (the spectra were calibrated with respect to the C 1s peak at 284.7 eV).

3.1.4 Fabrication of PPy NRs based chemo-resistive sensors

In order to observe the gas sensing properties of the PPy NRs ('sandwich structure' formation, see Figure 3.2) in chemo-resistive mode, the NRs were connected with top and bottom Ag electrodes (electrode gap: 8 mm) employing a commercial ink (Heraeus, AD1688-06). The top electrode was connected to the active layer (over deposited PPy film) and the bottom electrode to the Al substrate (Figure 3.3 a). Moreover, the substrates were glued to a hotplate in order to measure the gas response at different operating temperatures, if required (Figure 3.3 b). The delivery and mixing of gases were performed employing a mass flow system consisting computer-controlled mass-flow controllers. The sensors were tested towards different concentrations (25, 50 and 100, ppm) of nitrogen dioxide and ammonia in dry air by means of DC resistance measurements at RT.

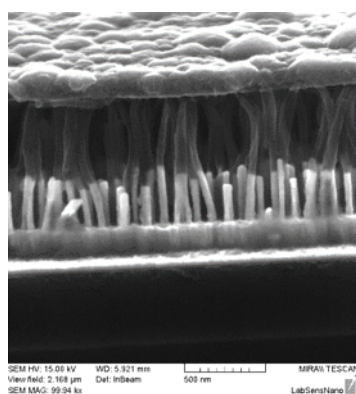


Figure 3.2: SEM image of PPy NRs with 'sandwich structure' formation

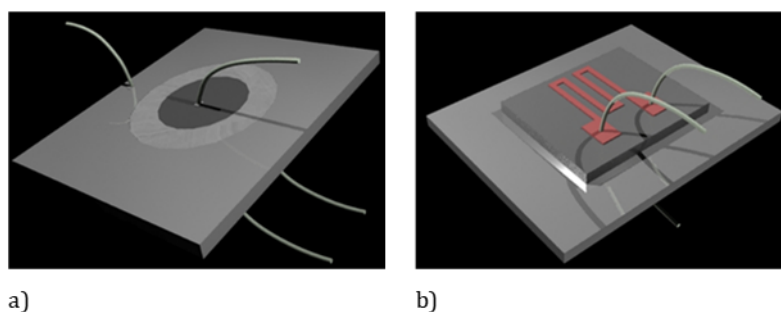


Figure 3.3: Schematic illustration of the chemo-resistive sensors: Deposition of the bottom-top Ag electrodes (a); Integration of the hotplate at the backside of the substrate (b).

3.2 Results

3.2.1 Physical and chemical characteristics of the PPy NRs and PPy NPs.

Figure 3.4 displays the morphology of the PPy NRs and PPy NPs observed via SEM and TEM, respectively. SEM of the PPy NRs (Figure 3.4 a) revealed quasi-aligned structures with a diameter of 50 nm and a length of 340 nm (grown on the top of 340 nm long Au NRs employed as template). TEM of the PPy NPs (Figure 3.4 b) proved the formation of homogeneously distributed compact spherical NPs with different sizes between 35 and 55 nm.

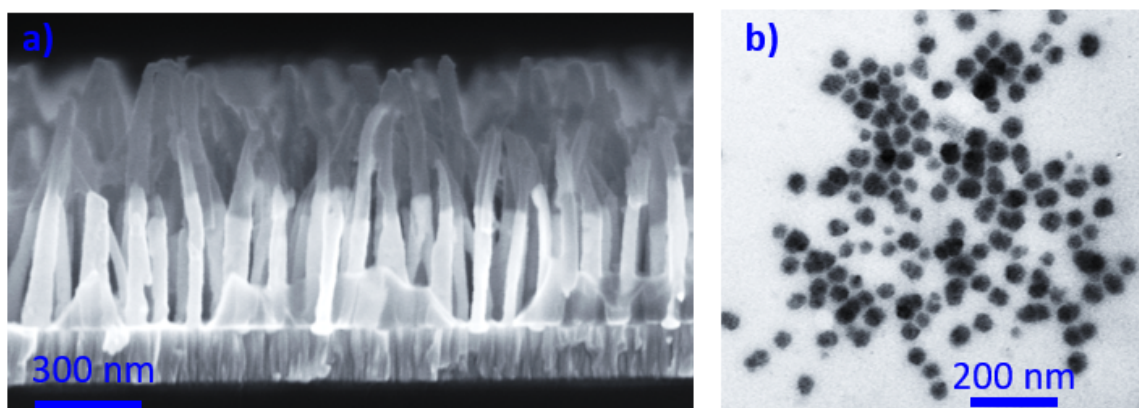


Figure 3.4: SEM and TEM images of the PPy NRs (a) and PPy NPs (b).

Raman analysis of PPy NRs and PPy NPs displayed various Raman bands between 620 and 1609 cm^{-1} , consistent with those reported previously in the literature for PPy based materials. Table 3.1 shows a summary of the Raman peaks observed in Figure 3.6 a, b with the assigned predominant band vibrations. Both samples displayed similar Raman bands with slight shifts of less than 20 cm^{-1} , most likely caused by the different laser wavelengths used for excitation of each sample.

Table 3.1: Assignment of Raman peaks for PPy NRs and PPy NPs in Figure 3.6.

Band	Wavenumbers, cm^{-1}	Assignment
A	620–626	C–C ring torsional
B	687–690	C–H wagging
C	933–939	C–C ring deformation (bipolarons)
D	963–985	C–C ring deformation (polarons)
E	1050–1056	C–H in-plane deformation (polarons)
F	1079–1084	C–H in-plane deformation (bipolarons)
G	1241–1253	Anti-symmetric C–H in-plane bending, ring stretching
H	1330–1333	C–C in-ring, anti-symmetric C–N stretching
I	1372–1389	C–C in-ring, anti-symmetric C–N stretching, C–H bending, N–H bending stretching
J	1492–1498	C–C, C=N stretching
K	1583–1609	C=C in-ring, C–C inter-ring stretching

XPS analysis showed characteristic C 1s and N 1s core level peaks both for the PPy NRs and PPy NPs which are consistent with the literature. After deconvolution into Gaussian components, the C 1s spectrum for the PPy NRs (Figure 3.5 a) films suggests the presence of four singlets. The peaks located at 284.2, 284.7, 286.3 and 288.6 eV can be attributed to β C atoms, α C atoms, =C–N $^{+}$ bond of PPy polarons and C=O bonds, respectively. Similarly, the C 1s core level peak recorded on the PPy NPs showed four components (Figure 3.5 b). Three of these components correspond to α carbon atoms, the =C–N $^{+}$ bond of PPy polarons, and the C=O species identified in the PPy NRs, whereas the fourth component at 287.7 eV corresponds to the –C=N $^{+}$ bond of bipolaron charge carrier species.

The N 1s core level peaks of PPy NRs (Figure 3.5 c) and PPy NPs (Figure 3.5 d) showed the presence of four and three components, respectively. The identified components are assigned to imine structure (=N– at 398 eV), neutral nitrogen in PPy ring (–N–H at 400.0 eV), polaron species of PPy (–N–H $^{+}$ around 401 eV) and bipolaron species of PPy (=N–H $^{+}$ around 402 eV).

Both samples (PPy NRs and PPy NPs) indicated a major presence of α carbon atoms in the PPy ring matching with the planar conformation of PPy (i.e., pyrrole rings linked by α -positions). However, the presence of β carbon atoms and deprotonated nitrogen atoms (=N–) in the PPy NRs (Figure 3.5 a, c) suggest a degree of disorder in this sample. This signifies a non-planar PPy configuration deviated from the ideal arrangement of PPy, in which pyrrole rings are linked only via the α -positions. The difference in PPy configuration between those two samples could be attributed to particular synthesis conditions such as reactants used for the synthesis.

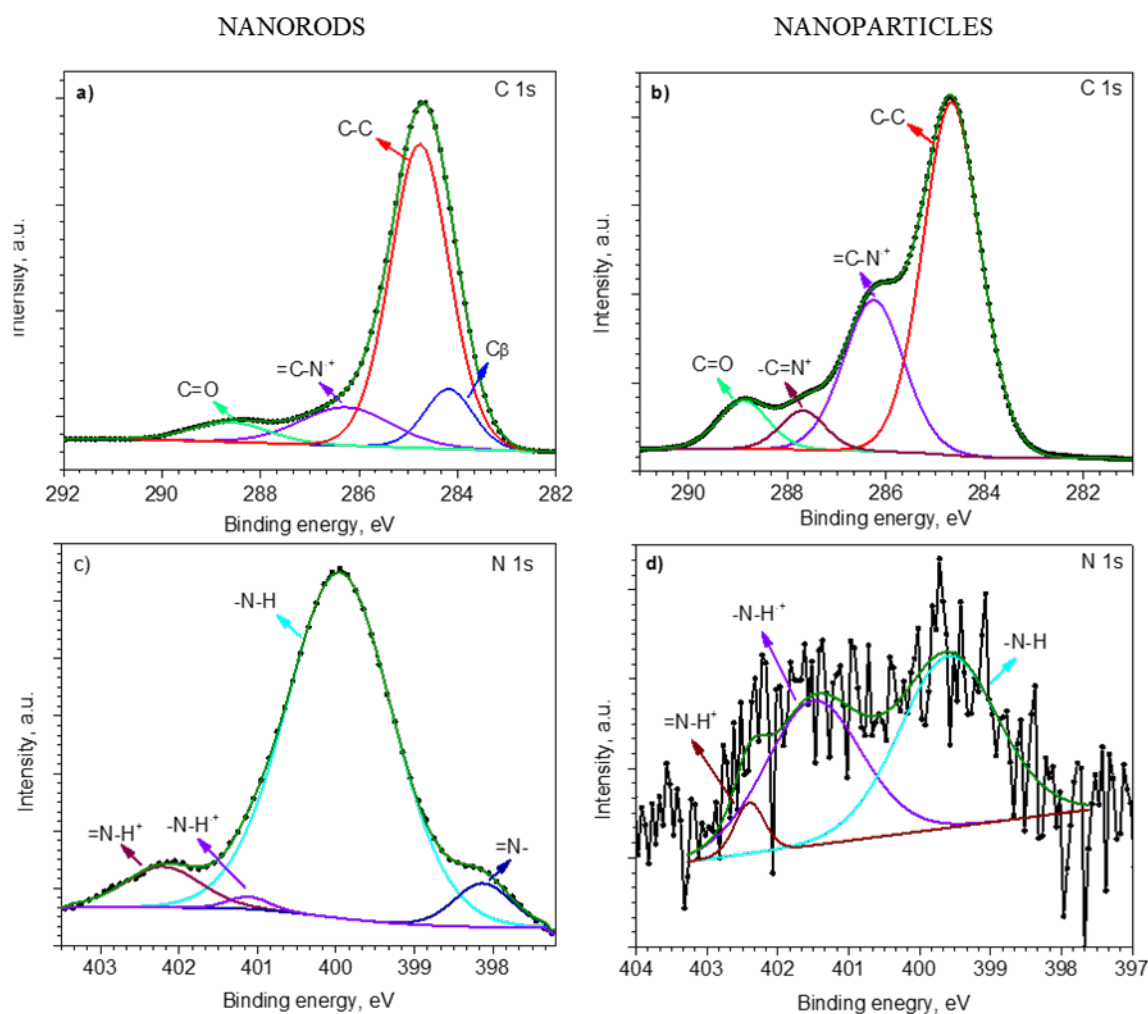


Figure 3.5: C 1s (a,b) and N 1s (c,d) XPS core level peaks recorded on the PPy NRs (left) and PPy NPs (right).

3.2.2 *In-situ* gas sensing test

To get an insight into the sensing properties of the PPy NRs and PPy NPs, the detection mechanism of PPy towards ammonia was investigated using *in-situ* Raman spectroscopy and XPS. Generally, the detection mechanism between PPy and ammonia occurs either via proton transfer (deprotonation) and/or electron transfer (electron injection).

Figure 3.6 a,b compare the Raman bands recorded before (reference spectra) and after exposing the PPy NRs and PPy NPs to ammonia (the characteristic Raman bands are labeled according to Table 3.1). The Raman bands (highlighted in green and yellow circles) in Figure 3.6 a,b showed significant changes in the intensity and the full width at half maximum (FWHM) with respect to the reference.

The column chart for the PPy NRs in Figure 3.6 c compares the relative change of area for each Raman band after ammonia exposure. The changes are particularly marked for the C, G, H, I and K vibration bands which display approximately 48, 64, 40, 72 and 55 % decrease in peak area after ammonia exposure, respectively. On the contrary, the D band is the only vibration band showing an increase in peak area and indicates a change of approximately 46 % after ammonia exposure. The observed changes of the characteristic Raman bands were assigned to the presence of a proton transfer and electron transfer mechanism in PPy NRs during ammonia exposure [174].

Further XPS analysis of the PPy NRs after ammonia exposure also confirmed the presence of an electron transfer mechanism. This mechanism was confirmed by an increase in relative area of polarons and simultaneous decrease of bipolarons species in the N 1s core level peak (Figure 3.7 a) after ammonia exposure. Similarly, the C 1s core level XPS spectrum after ammonia exposure also indicates an increase of =C-N⁺ (polaron) species (Figure 3.7 c). The presence of a proton transfer mechanism, as noticed

via Raman for the PPy NRs after ammonia exposure, was not evidenced in the XPS analysis, probably due to the different principles of XPS and Raman. XPS allows observing the chemical and/or electronic states of the elements at the material surface (up to 10 nm in depth) and Raman analyzes vibrational, rotational, and other low-frequency modes within the bulk of the material [174].

The changes on the Raman spectra of PPy NPs after ammonia exposure are also manifested by relative changes of area in each band (Figure 3.6 b,d). The most noticeable changes after ammonia exposure are observed for the bands C, I and J with a decrease in peak area of 64, 76 and 89%, respectively. In contrast, the D and H bands showed an increase in peak area of 77 and 53%, respectively. The changes in the C and D Raman bands for PPy NPs after ammonia exposure indicate a decrease in the amount of bipolarons (C band) with simultaneous increase of polarons (D band) which caused the formation of a new resonant structures in the pyrrole ring and in turn, the changes of other bands. Raman analysis confirmed the presence of the electron transfer mechanism between PPy NPs and ammonia [174].

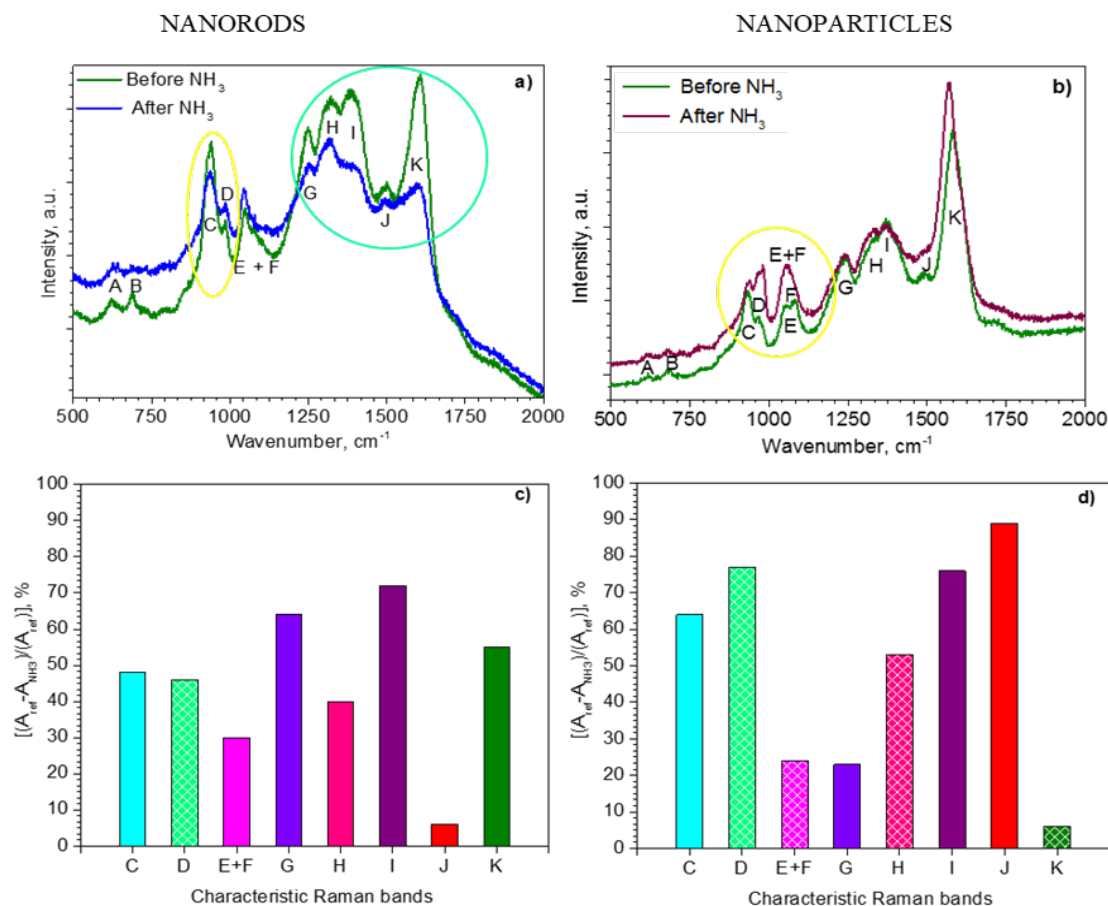


Figure 3.6: Raman spectra of the PPy NRs (a) and PPy NPs (b) before (green line) and after the exposure to ammonia (blue and brown line); Relative changes of each Raman band area $[(A_{ref} - A_{NH_3}) / (A_{ref})]$ for the PPy NRs (c) and PPy NPs (d) after ammonia exposure. The area of the corresponding band (i.e., C, D, E, etc.) before and after ammonia exposure is expressed by A_{ref} and A_{NH_3} , respectively. The patterned columns represent an increase in peak area after ammonia exposure, whereas the full color columns represent a decrease.

The N 1s core level spectrum also demonstrated the presence of positively charged nitrogen ($-N-H^+$) of polaron species, with a strong decrease in the bipolaron ($=N-H^+$) species and neutral nitrogen ($-N-H$) after ammonia exposure (Figure 3.7 b). These results indicate a nine-fold increase of the polarons to bipolarons ratio as compared to the ratio registered before ammonia exposure. The C 1s XPS core level spectra of the PPy NPs after ammonia exposure (Figure 3.7 d) also points out to the conversion of bipolarons into polarons. These results are consistent with the Raman analysis described above, indicating that the PPy NPs exposed to ammonia follow a detection mechanism dominated by electron transfer, with no evidence of a proton transfer mechanism as noticed for the PPy NRs [174].

In summary, these results indicate that the ammonia detection mechanisms in PPy are prone to be adjusted by the synthesis route, namely by tuning reactants, concentrations, and/or applied charge

density in the case of electrochemical deposition. These synthesis conditions at the first stage define the morphology, surface area and orientation of PPy. However, in a more advanced stage this influences the detection mechanisms of ammonia. Considering the specific synthesis conditions and gas analyte studied in this work, Raman and XPS tests evidenced electron transfer mechanisms in both, the electrochemically synthesized PPy NRs and the chemically synthesized PPy NPs, whereas the presence of detection mechanism in which protons are transferred was only evidenced in the case of PPy NRs.

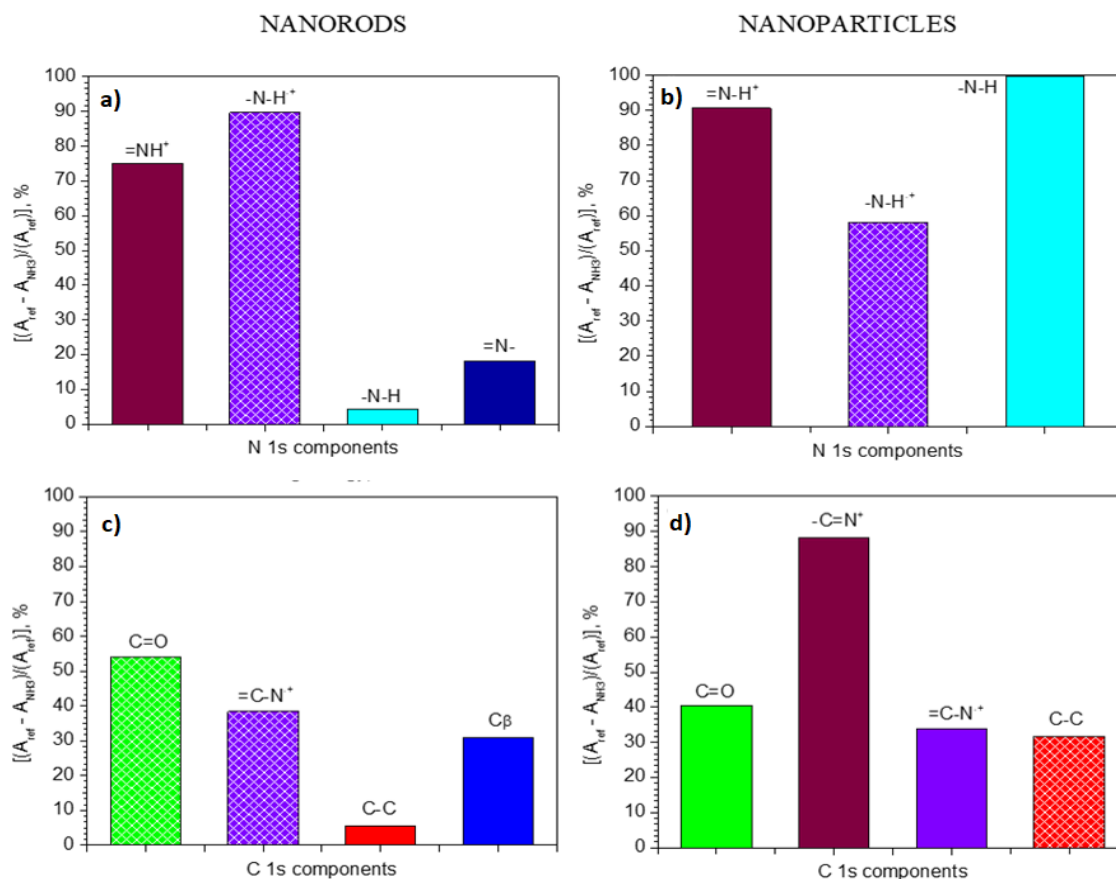


Figure 3.7: Relative change in area $[(A_{\text{ref}} - A_{\text{NH}_3})/(A_{\text{ref}})]$ of each N 1s core level component (NRs (a) and NPs (b)) and C 1s components (NRs (c) and NPs (d)) after ammonia exposure. The area of the corresponding components (i.e., $-N-H$, $-N-H^+$, C_β , $C-C$, etc.) before and after ammonia exposure is expressed by A_{ref} and A_{NH_3} , respectively. Patterned and full color columns represent an increase or decrease in peak area after ammonia exposure, respectively.

3.2.3 Ammonia and nitrogen dioxide test of PPy NRs based chemo-resistive sensors

PPy NRs based chemo-resistive sensors showed negligible resistance changes to nitrogen dioxide at both RT and higher operation temperature of 60 °C. Constant electrical resistance of 42 k Ω that changed to 39.5 k Ω after exposure to nitrogen dioxide without finding a steady state was observed at RT. Similarly, test to ammonia showed the same behaviour with negligible changes of the resistance. The negligible responses obtained to ammonia are inconsistent with the literature and previous Raman and XPS observations. The lack of response of chemo-resistive sensors based on PPy NRs with sandwich structure could be related to the architecture of the sensors with top and bottom electrodes (instead of only bottom electrodes) which impede the diffusion of the target gases and the acquisition of the electrical signal [175].

3.3 Conclusions

In-situ gas sensing test performed using Raman and XPS analysis suggested the potential of electrochemically synthesised PPy NRs and chemically synthesized PPy NPs to sense ammonia. Different sensing properties of those materials, for instance, the reaction mechanism between ammonia and PPy NRs (electron and proton transfer) and/or PPy NPs (electron transfer) appear to be connected to the particular morphological and chemical composition of each film. Electrochemically developed PPy NRs showed inadequacies for their application in gas sensor devices based on chemo-resistive transducing mode due to a complicated architecture caused by synthesis and post-synthesis integration processes, which results in negligible responses of sensor. Therefore, the obtained results moved the direction of this research to the use of PPy NPs as the sensing layer in the L-SAW gas sensors.

Chapter 4

Love wave sensors based on polypyrrole modified with catalytic metal nanoparticles

Due to the complexity to fabricate functional sensing devices based on PPy NRs and the poor sensitivity observed in the preliminary studies discussed in previous chapter, the fabrication and tests of PPy were directed to the use of PPy NPs due to their simple synthesis and easy implementation with the electronic system using different coating techniques (e.g., spin coating, drop coating). In Section 2.1 it was found that the use of hybrid sensing materials ensures the development of gas sensors with enhanced sensing performances. As there is a lack of literature reports related to SAW sensors (especially those with L-SAW principle) based either on bare PPy or PPy modified with other materials (e.g., metallic particles), their development was investigated in this thesis. This chapter describes the fabrication of L-SAW sensors based on non-modified PPy NPs and PPy NPs modified with Au and Ag NPs, and their gas sensing tests toward the target gases. These outputs are associated to specific objective 3 and 4 in this thesis, and they were published in a journal articles, *Love wave sensors based on gold nanoparticle-modified polypyrrole and their properties to ammonia and ethylene* [176] and *Love Wave Sensors with Silver Modified Polypyrrole Nanoparticles for VOCs Monitoring* [177].

4.1 Experimental

4.1.1 Synthesis of Au/PPy

Colloid Au NPs were synthesized by the reduction of Au salt by sodium citrate. Briefly, 20 mL of 1 mM of gold (III) chloride trihydrate ($\text{HAuCl}_4 \cdot 3\text{H}_2\text{O}$) was added to a flask and placed on a stirring hotplate at 150 °C. As soon as the solution reach its boiling point, 2 mL of 1 % sodium citrate dihydrate ($\text{Na}_3\text{C}_6\text{H}_5\text{O}_7 \cdot 2\text{H}_2\text{O}$) was added and temperature was decreased to 100 °C. The reaction was run until the solution became reddish. Afterwards the solution was removed from the hotplate and cool down.

The solutions of Au NPs and PPy NPs (preparation described in Section 3.1.2) were mixed with two different ratios, 1:10 and 1:2 in order to create Au/PPy mixture.

4.1.2 Synthesis of Ag/PPy

Ag NPs were synthesized by a chemical reduction of silver nitrate (AgNO_3) with sodium borohydride (NaBH_4). Briefly, 10 ml volume of 1 mM AgNO_3 was added drop wise (about 1 drop/second) to 30 mL of 2 mM NaBH_4 solution that had been chilled in an ice bath. The reaction mixture was stirred vigorously on a magnetic stir plate. After the addition of all AgNO_3 , the mixed solution turned light yellow and the stirring was stopped after 10 min.

The Ag/PPy solution consisted of a mixture of Ag NPs and PPy NPs in a volumetric ratio of 1:10 since we noticed from Au/PPy experiment that this relation of catalytic metal and polymer is adequate for both the uniform coating and the sensing properties.

4.1.3 Fabrication of L-SAW sensor

L-SAW delay line platforms consisting of a piezoelectric substrate (ST-90°X quartz, 9 mm×4 mm×0.5 mm) with two (input/output) aluminium IDTs (200 nm thick) ports, see Figure 4.1. The double finger pair IDTs have four strips per period ($\lambda=28 \mu\text{m}$) and this structure is repeated 75 times for each port. The IDTs aperture and distance between IDTs ports (delay line) are 2.1 mm. In this work, a multi-guiding layer structure, in which the first guiding layer consisted of SiO₂ (3 nm thick) and the second guiding layer of a gas sensitive conductive polymer, was employed.

Regarding the second guiding/sensitive layers, two different series of L-SAW sensors were developed. First, the PPy and/or Au/PPy solution were spin-coated over the first (SiO₂) guiding layer at a speed of 4000 rpm and acceleration of 4000 rpm/sec for 1 min in order to create the second guiding/sensitive layers. Three types of L-SAW sensors (PPy, Au/PPy (1:10) and Au/PPy (1:2)) were fabricated.

In second case, the guiding/sensitive layers of L-SAW is based on PPy and/or Ag/PPy. These layers were spin coated at a velocity of 2500 rpm and acceleration of 2500 rpm/sec for 1 min. Two types of L-SAW sensor (PPy, Ag/PPy (1:10)) were developed.

To control the reproducibility of the spin coating, the L-SAW substrates were placed into a customized holder built to keep the substrates in a fix position and alignment during the coating.

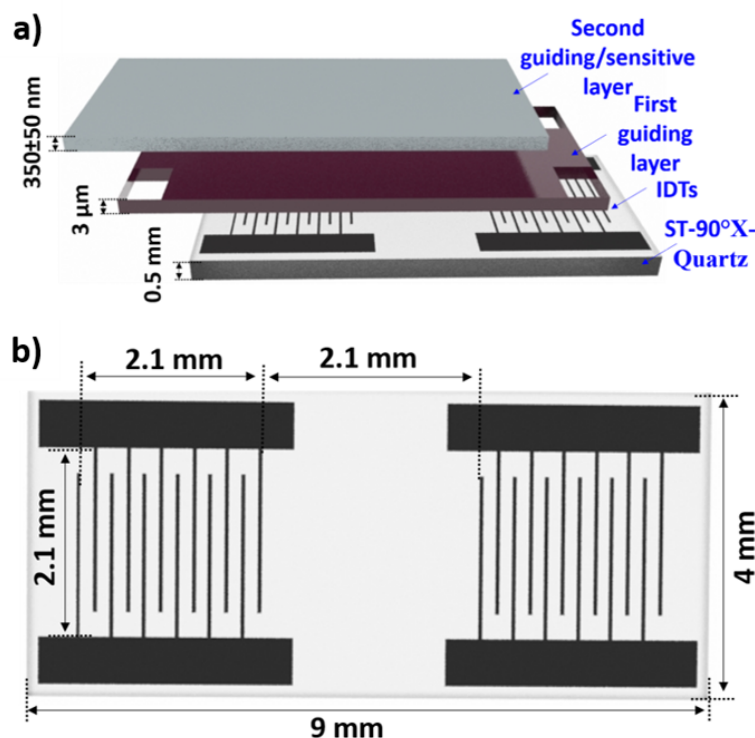


Figure 4.1: Schematic view of the L-SAW sensing element.

4.1.4 L-SAW sensors characterization

The morphology and chemical composition of PPy based gas sensitive materials were investigated using a high-resolution transmission electron microscope (HR-TEM, FEI TITAN Themis 60–300 kV), SEM equipped with focus ion beam (FIB/SEM, Helios G4 NanoLab DualBeam), XPS (Kratos Axis Supra) and Time-of-Flight Secondary Ion Mass Spectrometry (ToF-SIMS, TOF.SIMS5, Ion-ToF). The electrical characterization and measurements of the transmission scattering parameter (S_{21}) were performed using a network analyzer (Agilent 4395A).

4.1.5 Gas sensing tests

The gas sensing properties of the first series of L-SAW sensors (PPy and Au/PPy) were tested toward various ethylene (Praxair) and ammonia (Praxair) concentrations (2, 5 and 10 ppm). The sensors were exposed to each analyte for 2 min and purified with dry or humid synthetic air for 30 min.

The second series of L-SAW sensors based on PPy and Ag/PPy were tested toward acetone (Praxair, 100 ppm), ethanol (Praxair, 100 ppm) and toluene (Praxair, 200 ppm) in concentration range from 0.5 to 5 ppm. These sensors were exposed to each analyte for 2 min and purified with dry or humid synthetic air for 10 min.

Gas sensing tests of the all L-SAW sensors were carried out simultaneously in a continuous gas flow test chamber equipped with mass flow controllers at RT (24 °C) and both, in dry and humid environments with 10 and 30% RH. Both, temperature and humidity were monitor inside the test chamber using a humidity/temperature sensor (SHT71, operating ranges from 0 to 100 % RH, accuracy of ± 3 % RH).

Each L-SAW sensor works in an oscillator circuit, which includes an amplifier and a directional coupler. Therefore, the oscillating frequency of the sensor is shifted for any perturbation. A heterodyne configuration was used for signal acquisition, mixing the signal of the oscillator coupled to a reference L-SAW sensor (with only SiO₂ guiding layer) and the signal of the oscillator coupled to the PPy based L-SAW sensor. The frequencies obtained from the mixer were acquired by a frequency counter. The reference L-SAW sensor was used in the gas sensing array, to compensate thermal and other environmental dependent drifts on the piezoelectric substrates. During the gas test, the reference element was not exposed to target gas analytes, and the final output signal of the L-SAW sensors was subtracted from the reference sample. Therefore, the sensor response was defined as the frequency shift, which is the divergence of sensors frequency read off during the exposure to synthetic air and gas.

4.2 Results

4.2.1 PPy and Au/PPy L-SAW sensors

The morphological analysis demonstrated the synthesis of both PPy and Au NPs, and they incorporation in the mixture (Au/PPy). The properties of PPy NPs were described above (Section 3.2.1). HR-TEM analysis of the Au/PPy NPs (Figure 4.2 a) displayed the presence of segregated PPy and Au spherical particles; notice the brightness/contrast differences, which indicate the presence of both, Au (higher contrast) and PPy (low contrast) NPs. The number of PPy NPs were remarkably larger in comparison to the Au NPs in tested sample, confirming the relatively low amount of Au NPs in the Au/PPy mixture. The average particle size analysis indicates that the mean diameter of Au NPs is approximately 15 nm for a size distribution ranging between 12 and 25 nm. HR-TEM of the Au NPs emphasized their high crystallinity showing lattice fringe spacing of 0.24 nm (Figure 4.2 b). This is consistent with the (111) plane of the face centred cubic (fcc) gold ($d=2.35500$ Å, ICDD card no. 04-0784).

SEM (Figure 4.2 c) analysis of the Au/PPy second guiding/sensitive layers, after spin coating of the L-SAW transducing platforms, displayed uniform films with granular morphology. The films proved good adhesion to the substrate and the thickness of the films observed by cross-sectional SEM images (see Figure 1b) was found to be 350 ± 50 nm.

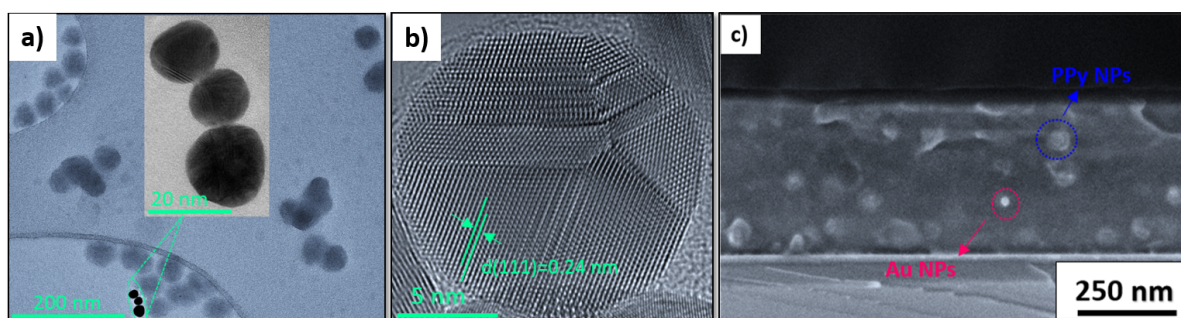


Figure 4.2: HR-TEM images of the Au/PPy NPs (a) with close view on the Au NPs (b); SEM-image of the PPy guiding/sensitive layer modified with Au NPs after spin coating (c); notice the difference in brightness/contrast of the PPy grains and the Au NPs.

The incorporation of the Au NPs into the spin coated guiding/sensitive layers in the samples (PPy, Au/PPy (1:10) and Au/PPy (1:2)) were also investigated by TOF-SIMS technique. The obtained results demonstrated the presence of characteristic fragmented ions of Au⁻ at 196.97 m/z in the Au/PPy samples, in contrast to the bare PPy samples. The correlation of the Au⁻ ion intensity and Au NPs loadings in the samples confirmed the proportional increase of Au⁻ signal with respect to the Au NPs amounts

introduced to the samples. Au⁻ ion intensity for PPy, Au/PPy (1:10) and Au/PPy (1:2) was 0, 0.2 and 1, respectively [176].

The electrically characterized of PPy, Au/PPy (1:10) and Au/PPy (1:2) L-SAW sensors displayed very similar response for all tested sensors, with the operation frequency and the insertion loss of 161.6 ± 0.4 MHz and 22.4 ± 0.5 dB, respectively.

The ammonia and ethylene gas sensing tests of the L-SAW sensors based on PPy and Au-modified PPy NPs (1:10 and 1:2) at RT are presented in Figure 4.3. In general, all sensors registered positive responses upon exposure to different concentrations of target analytes. The sensors based on Au/PPy demonstrated enhanced sensing properties towards both tested gases compared to the sensors based on non-modified PPy NPs. The sensors based on low Au loadings (i.e., 1:10) provided better responses to ammonia (Figure 4.3 a) compared to those based on high Au loadings (i.e., 1:2). Namely, Au/PPy (1:10) sensors showed higher frequency shifts and an increase of the response by approximately 5, 4 and 3 times to 2, 5 and 10 ppm of ammonia, respectively, as compared to PPy sensors. In contrast, the results obtained for ethylene (Figure 4.3 b) registered improved responses for Au/PPy (1:2) sensor (higher Au loading) compared to Au/PPy (1:10) sensor, as opposite to that observed for the ammonia tests. The frequency shifts of Au/PPy (1:2) sensors with regard to non-modified PPy sensors is increased approximately by 4 times for 2, 5 and 10 ppm of ethylene.

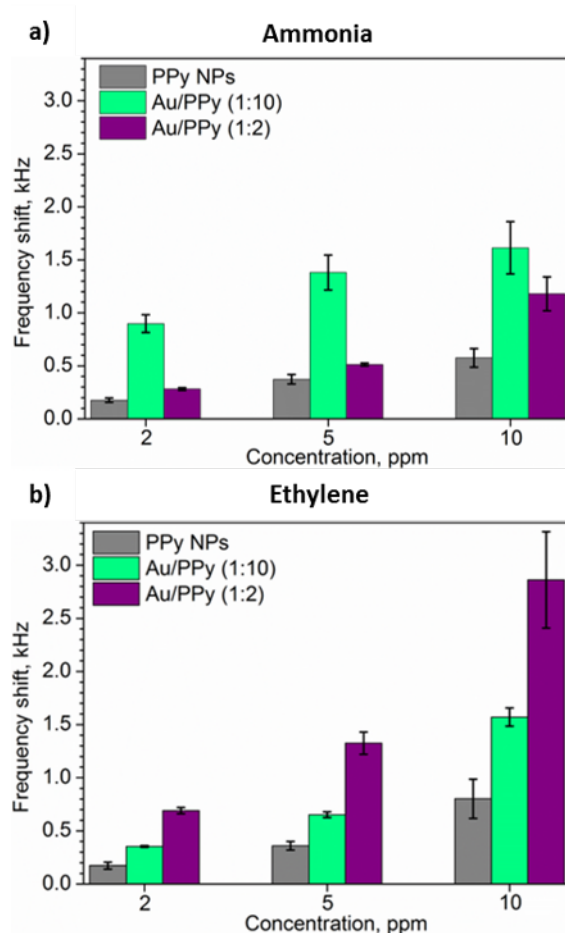


Figure 4.3: Frequency shifts recorded on the non-modified PPy and modified PPy L-SAW sensors with low (1:10) and high (1:2) Au loadings at 2, 5 and 10 ppm of ammonia (a) and ethylene (b).

The Au/PPy (1:10) and Au/PPy (1:2) sensor showed increased sensitivity to ammonia and ethylene, respectively. The response and recovery times of Au/PPy (1:10) sensors to 5 ppm of ammonia were 59 s and 72 s, respectively, and 81 s and 142 s for Au/PPy (1:2) sensors to 5 ppm of ethylene. The LOD for ammonia was 67 ppb using Au/PPy (1:10) and for ethylene 87 ppb using Au/PPy (1:2) sensors, considering that the minimum signal intensity is 3 times higher than noise. When Au/PPy L-SAW sensors were tested to ethylene and ammonia in humid ambient, a loss of the response of approximately 2 times at 10 % RH and 5 times at 30 % RH were registered.

In summary, the incorporation of the second guiding/sensitive layers with the piezoelectric substrates demonstrates similar morphological and electrical properties for the non-modified and Au modified PPy layers, despite the two different Au loadings incorporated in the modified layers. The Au-modified PPy L-SAW sensors demonstrate enhanced sensing responses compared to the non-modified PPy sensors in dry conditions, with better sensitivity and lower LOD to ethylene and ammonia. The tests in humid ambient affect the sensor performance modifying the responses to lower magnitude than those obtained in dry ambient, thus, indicating the need for further strategies to compensate the interference of humidity on the sensor response.

4.2.2 PPy and Ag/PPy L-SAW sensors

As the morphology and chemical analysis of PPy NPs were mentioned above (Section 3.2.1), this section includes the properties of Ag NPs. The synthesis of crystalline Ag NPs was corroborated by HR-TEM. Figure 4.4 a displays the TEM images of the particles with mean diameter of approximately 17 ± 3 nm (calculated for a population of 30 particles) and lattice fringes with spacing of ~ 0.23 nm, consistent with the (111) planes of Ag face centered cubic phase (JCPDS number 04-0783). High-resolution XPS analysis of the Ag NPs (Figure 4.4 b) revealed typical Ag 3d doublets separated by 6 eV. The SEM study of the PPy and Ag/PPy NPs guiding/sensitive layers after spin coating showed the integration of uniform sensing layers with a thickness of $\sim 262\pm 10$ nm on the L-SAW platforms. A typical cross-section SEM image of the L-SAW sensors is displayed in Figure 4.4 c.

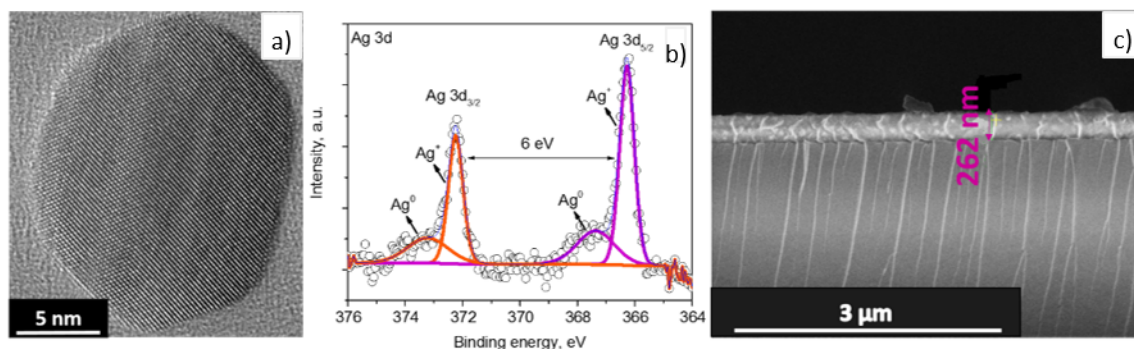


Figure 4.4: HR-TEM image of the Ag NPs (a); High resolution XPS spectra of the Ag 3d core levels at the Ag NPs (b); Typical cross-section SEM image of the L-SAW sensors after spin coating of PPy or Ag/PPy NPs (c).

The PPy and Ag/PPy L-SAW sensors were characterized by measuring of S_{21} parameter, the results showed the similar response for both sensors with the resonance frequency of 161.6 ± 0.1 MHz and the insertion loss of 19.7 ± 1 dB.

The calibration curves of PPy and Ag/PPy L-SAW sensors for acetone, ethanol and toluene are shown in Figure 4.5 a,c,e, respectively. These figures show the proportional increase of the sensor response with the increase of concentration for each gas. Generally, the results display enhanced responses for the Ag/PPy sensors compared to the PPy sensors for all tested gases, with frequency shifts of approximately 1.4 times more for the Ag/PPy sensors than for the PPy sensors. These results are in line with observation for Au/PPy sensors, which proved the enhancement of gas sensing properties (e.g., sensors response) by the modifications of a host gas sensitive material with metal catalysts (e.g., Ag, Au). Ag/PPy sensors exhibited a higher sensitivity to acetone than to ethanol and toluene, which register a cross-sensitivity respect to acetone of 81% and 37%, respectively. These results indicate a relatively low interference among tested analytes.

The LOD of the Ag/PPy L-SAW sensors was estimated to be 3, 5 and 20 ppb for acetone, ethanol and toluene, respectively. These LOD are below the limits set for acetone, ethanol and toluene in different areas (see Section 2.4). For instance, the TLV for acetone, ethanol and toluene are 250, 1000 and 20 ppm, respectively. Similarly, the concentration of VOCs in the food industry are above (typically by tens or hundreds of ppb) the LOD obtained for these L-SAW sensors. Additionally, in the breath analysis field, the concentrations of acetone, ethanol and toluene in the exhaled breath (e.g., lung cancer patients register concentrations of 112–2654 ppb of acetone, 13–1520 ppb of ethanol and 9.3–21.3 ppb of toluene) are above the LOD obtained in this work.

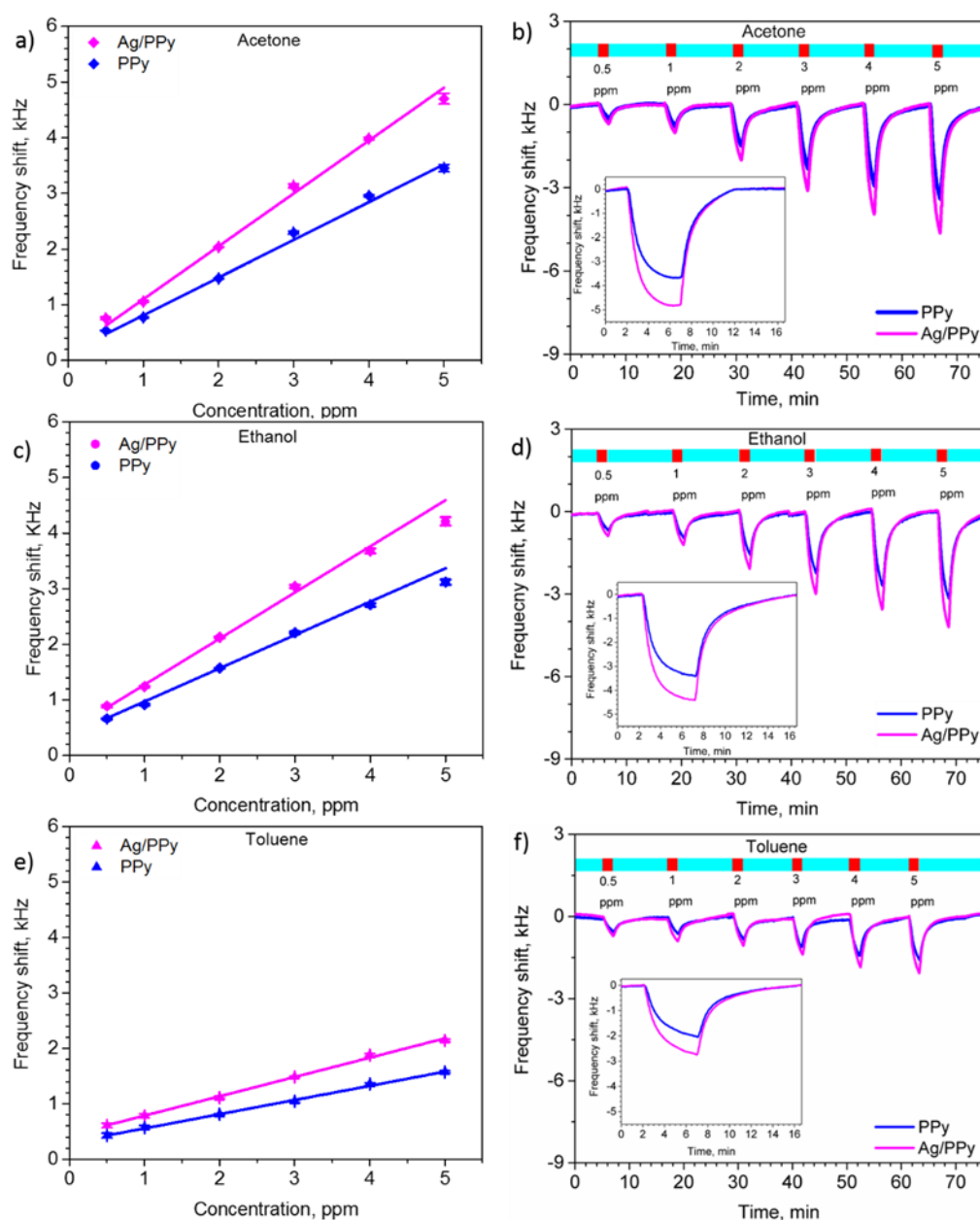


Figure 4.5: Calibrations curves and dynamic responses of the L-SAWsensors (based on PPy and Ag/PPy) for acetone (a,b), ethanol (c,d), and toluene (e,f). The insets in (b,d,f) display the time dependent response to 5 ppm of each gas.

The dynamic response of the PPy and Ag/PPy L-SAW sensors exposed to various concentrations of acetone, ethanol and toluene are presented in Figure 4.5 b,d,f, respectively. One can notice from these results that the Ag/PPy and PPy sensors displayed stable and reversible responses. The results showed that the response and recovery time for the Ag/PPy sensors was approximately 10 s faster than that for the PPy sensors. This could be attributed the catalytic properties of chemically active Ag NPs, which accelerate the gas-solid interactions at the guiding/sensitive film. The response times for the Ag/PPy sensors to acetone and ethanol were below 2.5 min, and below 3.5 min for toluene. In addition, the Ag/PPy sensors required less than 4 min to recover after acetone exposure and less than 5.5 min after ethanol and toluene exposure.

Similar to Au/PPy sensors, the humid environment had critical effect on the response of Au/PPy sensors. For instance, the sensor response to 5 ppm of acetone decreases by a factor of 2 and 7 when the atmosphere changes from dry to 10 % and 30 % RH, respectively. The loss of response in the Ag/PPy sensors in a humid atmosphere may be caused by the water vapor sorption into the polymer layer, which fills the free volume fraction in the polymer and reduces the gas permeability. This is a common issue in

polymer based gas sensors that needs further technological solutions such as the use of humidity filters or dehydration elements in order to exploit these sensors in future consumer devices [177].

In summary, the above results suggest that PPy functionalization using Ag NPs enhances the response, sensitivity and speed of L-SAW sensors to organic vapors, particularly to acetone. A moderate response to acetone was registered by running the tests in humid conditions (10 % and 30 % RH) with the sensors detecting concentrations down to 1 ppm. Overall, these results demonstrated enhanced properties of Ag/PPy L-SAW sensors, providing a technological solution for monitoring low concentrations of VOCs at RT.

4.3 PPy NPs chemo-resistive sensors

For comparison purposes, PPy, Au/PPy and Ag/PPy layers were integrated with chemo-resistive traducing platforms using the same preparation procedure as for the deposition of those sensitive layers in L-SAW sensors, i.e. spin coating. The sensors were tested to 80 ppm of ethanol. The sensors showed extremely high resistance in $G\Omega$ range with the difficulty to be measured with the standard equipment. Only Au/PPy sensors showed response to ethanol which was measurable.

4.4 Conclusions

In summary, the selection of PPy NPs as a primary gas sensing material of investigation together with the simple and repeatable fabrication of micro sensing elements based on L-SAW principle turned out to be the right decision. The obtained results showed the positive response of the fabricated sensors to all target gases. High response of PPy based L-SAW sensors to low concentration (in ppb levels for acetone, ethanol and toluene) at RT met the expectations which were set up in the beginning of this thesis. Generally, the sensors based on organic-inorganic hybrid materials showed the enhanced sensing performances over non-modified (bare PPy). Therefore, the further direction of this thesis was established on exploring new PPy nanocomposites and their implementation in L-SAW sensors, as the last proved better sensing properties over chemo-resistive sensors.

Chapter 5

Love wave sensor based on polypyrrole modified with CdTe quantum dots

Nanocomposite (inorganic-organic) materials have attracted a widespread attention in the field of gas sensing by many researches, as an alternative solution to overcome the limitations of single counterparts and to improve the final sensing properties. The various combinations of inorganic-organic materials were reported, for instance, CPs (e.g., PPy) were mixed with noble metals, MOXs, graphene etc. However, the modification of either PPy or others CPs with semiconductor QDs and their implementation into gas sensing platforms gained small attention in previous research, even though QDs showed an outstanding opto-electronic features together with large surface area due to their small size. Therefore, the further objective of my doctoral study was directed to synthesize inorganic-organic nanocomposites based on CdTe/PPy and integrate them with L-SAW. The obtained results are associated to specific objective 3 and 4 of this thesis, and they are summarized in the article “*Cadmium telluride/polypyrrole nanocomposite based Love wave sensors highly sensitive to acetone at room temperature*”. This article is under review since 08.05.2020 in the *Sensors and Actuators B: Chemical*.

5.1 Experimental

5.1.1 Synthesis of CdTe QDs

The synthesis of CdTe QDs capped with mercaptopropionic acid (MPA) was realized according to previous procedure [178]. In the first step, Cd-MPA solution was prepared using cadmium chloride (CdCl_2 , 183 mg) and tri-sodium citrate dihydrate ($\text{HOC}(\text{COONa})(\text{CH}_2\text{COONa})_2 \cdot 2\text{H}_2\text{O}$, 400 mg) dissolved in deionized water (100 ml), whereupon MPA ($\text{HSCH}_2\text{CH}_2\text{CO}_2\text{H}$, 104 ml) was added. Sodium hydroxide (NaOH , 1 M) was used to adjust the pH of the Cd-MPA solution to 10, and subsequently, sodium tellurite (Na_2TeO_3 , 44 mg) and sodium borohydride (NaBH_4 , 100 mg) were added. The mixed solution was heated up to 95 °C and the reaction to form CdTe QDs was carried out using a reflux cooling system for 4 h. Afterwards the QDs were purified using isopropyl alcohol and centrifugation process for one cycle. The CdTe QDs were then dried and stored in fridge.

CdTe/PPy nanocomposite was prepared by mixing PPy NPs and CdTe QDs (concentration of 30 mg/ml) aqueous solutions in volumetric ratios of 1:10 and 1:2.

5.1.2 L-SAW sensor fabrication

The fabrication procedure of multi-guiding CdTe/PPy L-SAW sensors was the same as for Au/PPy (see Section 4.1.3). The second guiding/sensitive layers were spin-coated at a speed of 4000 rpm and acceleration of 4000 rpm/sec for 1 min. Three L-SAW sensors including CdTe/PPy (1:10), CdTe/PPy (1:2), and non-modified PPy layers were investigated.

5.1.3 Characterization of sensing materials

The various microscopy (HR-TEM, Atomic force microscopy (AFM, Dimension Icon, Bruker)) and spectroscopy (XPS, Fourier transform infrared spectroscopy (FTIR, Vertex70, Bruker)) techniques were

used to investigate the morphological and structural properties of the sensing layers. The electrical properties of CdTe/PPy sensors were also determined.

5.1.4 Gas sensing test

The gas sensing test of CdTe/PPy sensors were carried out using the same condition and electronic equipment as for Ag/PPy sensors (see Section 4.1.5). The sensors were tested toward acetone, ethanol and toluene in concentration range from 0.5 to 5 ppm in dry and humid environment. To get an insight into the possible reaction mechanisms to acetone, the sensing properties of the L-SAW sensors were also investigated using FTIR before and after exposing the sensors to this analyte for 10 min.

5.2 Results

5.2.1 Characterization of the sensitive materials

The morphological and structural characteristics of the PPy NPs, CdTe QDs and CdTe/PPy nanocomposites were investigated by TEM, and the distribution of elements in the composite sample was explored using energy dispersive X-ray (EDS) analysis. Figure 5.1 a displays the amorphous PPy NPs. Figure 5.1 b demonstrates the crystalline CdTe QDs (marked by green circles) with average sizes of 3.1 ± 0.7 nm and interplanar spacing between lattice fringes of ~ 0.37 nm, consistent with lattice spacing of the (111) plane of cubic CdTe ($d = 0.374$ nm, JCPDS card No. 15-0770). The TEM and EDS mapping images of the CdTe/PPy nanocomposite are presented in Figure 5.1 c and Figure 5.1 d. These images demonstrate the random distribution of small QDs clusters (4.4 ± 0.8 nm) with a tendency to adhere to the PPy NP surface. The EDS mapping corroborates the characteristic PPy elements (i.e., C, N) distributed over the PPy NP area (big particle), while the typical elements for the CdTe QDs (i.e., Te, Cd) are detected only at the outer edge of the PPy NPs (small particles); only Te was evident by EDS.

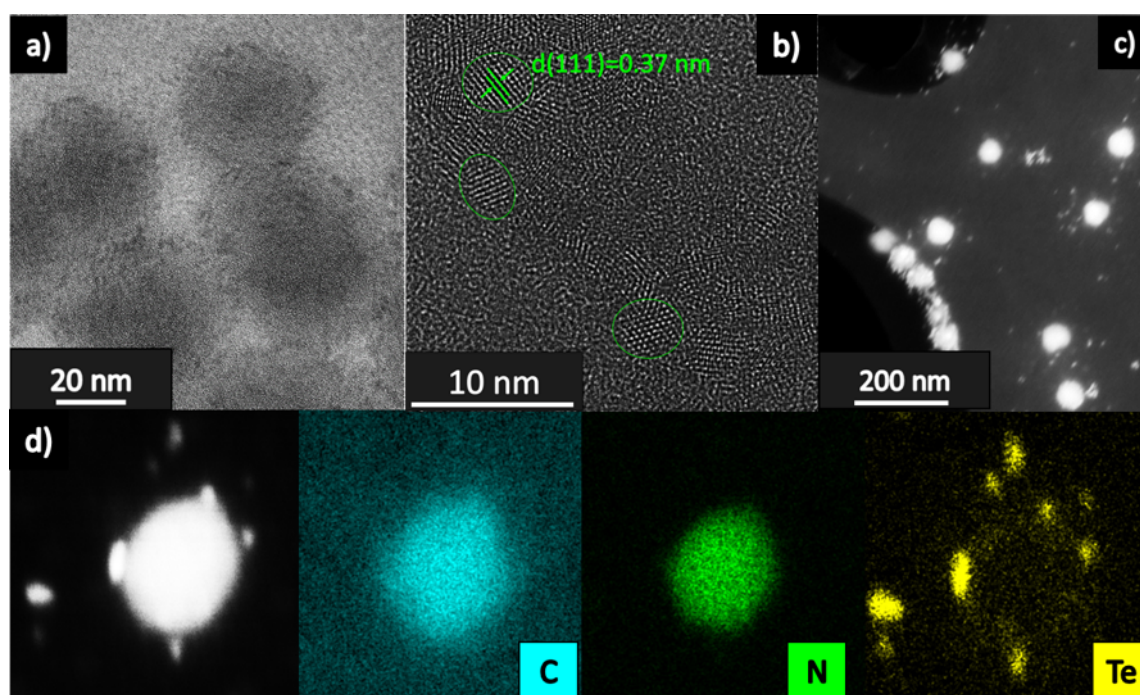


Figure 5.1: TEM image of the PPy NPs (a). HR-TEM image of CdTe QDs (b). TEM image of the CdTe/PPy nanocomposites (c). TEM and corresponding EDS elemental mapping images of the CdTe/PPy nanocomposites (d).

The chemical characterization techniques (FTIR and XPS) used for analysis of PPy and CdTe/PPy layers confirmed the creation of a blend of PPy NPs with PVA after the oxidative chemical polymerization of pyrrole monomer. The results also proved the incorporation of CdTe QDs in the spin coated sensitive

PPy layers. TEM, FTIR and/or XPS analysis identify both PPy and CdTe in the nanocomposites indicating no chemical interaction between them.

Electrical characterization of the PPy, CdTe/PPy (1:10) and CdTe/PPy (1:2) L-SAW sensors were investigated by measuring their transmission scattering parameter (S_{21}). The magnitude of the insertion loss versus the resonant frequency of the sensors for the reference (i.e., with only SiO₂ guiding layer) and the L-SAW sensors (with the second sensitive/guiding layer based on PPy or CdTe/PPy) is displayed in Figure 5.2. The results showed the shift in the resonant frequency from 165.3 MHz (reference sensor) to 162.5 MHz for the PPy, 162.4 MHz for the CdTe/PPy (1:10), and 163.7 MHz for the CdTe/PPy (1:2) L-SAW sensors. An increase of the insertion loss from -18 dB (reference sensor) to -22 dB (PPy and CdTe/PPy (1:10) sensors) and even to -32 dB in the case CdTe/PPy (1:2) sensors is also observed. The changes in operation frequency of the L-SAW sensors may be attributed to the confinement of the acoustic energy by the second guiding/sensitive layer. However, the larger differences in frequency and insertion loss for the CdTe/PPy (1:2) compared to the other L-SAW sensors could be caused in major degree by the parameters of the sensitive layer, including its thickness, density, or shear stiffness. Profilometry measurements corroborated this fact as the sensitive layers revealed more than two times higher thickness (250 nm) for the PPy and CdTe/PPy (1:10) L-SAW sensors as compared to the CdTe/PPy (1:2) L-SAW sensors (100 nm). Normally, L-SAW sensors with thin sensitive/guiding layers (of the same nature) involve lower insertion loss compared to thick layers [179]. However, this is not the case for the CdTe/PPy (1:2) L-SAW sensors, which despite the lower thickness respect to the CdTe/PPy (1:10) layer, register higher insertion loss due to the higher concentration of QDs and their tendency to agglomerate. AFM analysis confirmed this fact, showing the irregular agglomeration of QDs over the sensitive layer surface of the CdTe/PPy (1:2) L-SAW sensor. This was not noticed in the case of CdTe/PPy (1:10) L-SAW sensor.

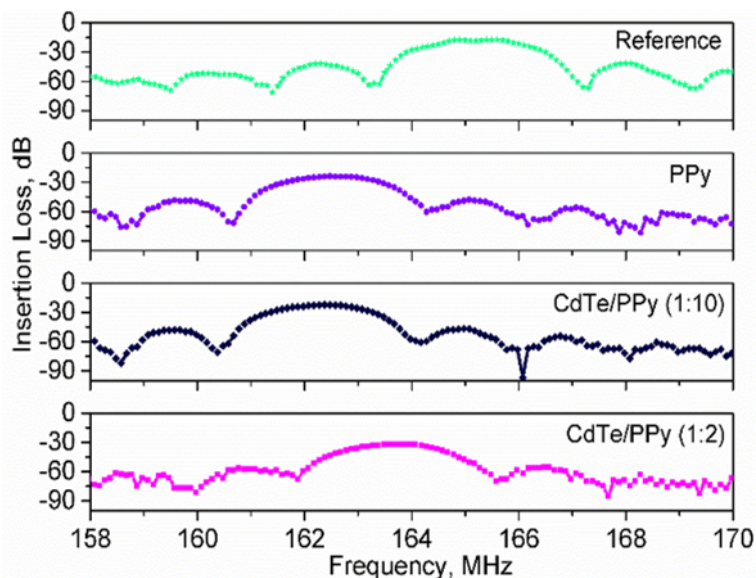


Figure 5.2: Transmission scattering parameter (S_{21}) for the reference, PPy, CdTe/PPy (1:10) and CdTe/PPy (1:2) L-SAW sensors.

5.2.2 Gas sensing test

The following studies were employed to characterize the PPy, CdTe/PPy (1:10) and CdTe/PPy (1:2) L-SAW sensors and to examine the effects of the CdTe QDs in the gas sensing properties of PPy. To this end, the gas sensing test of the sensors toward acetone, ethanol and toluene were explored at RT. The frequency response of the sensors to 5 ppm of acetone is shown in Figure figure 5.3. Generally, the L-SAW sensors with low QD loadings (CdTe/PPy (1:10)) displayed the highest response among the three type of sensors, whereas the sensors with the higher QD loadings (CdTe/PPy (1:2)) showed the lowest responses. Thus, the response amplitude of the CdTe/PPy (1:10) sensors to acetone was 1.2 and 2 fold higher than that of PPy and CdTe/PPy (1:2) sensors, respectively. The L-SAW sensors responses to ethanol and toluene were in the same order as for acetone, with the highest and lowest frequency shifts with respect to the PPy sensors being observed for CdTe/PPy (1:10) and CdTe/PPy (1:2) sensors, respectively.

These results and, analogously, the previous studies of Au/PPy and Ag/PPy L-SAW sensors prove the enhancement of PPy sensing properties by the incorporation of inorganic catalytic particles. Overall, we notice that the use of relatively low amounts of QDs (CdTe/PPy (1:10)) in the second/guiding PPy sensitive layer decreases the velocity of the acoustic wave without modifying significantly the total losses of the system. This allows for boosting the response and enhancing the functional properties of the whole sensor. Additionally, the operating frequencies of PPy and CdTe/PPy (1:10) sensors in the same range, indicate that the enhanced properties of the CdTe/PPy (1:10) samples are also connected to the incorporation of CdTe QDs in PPy. In contrast, the use of high amounts of QDs, which tend to agglomerate the CdTe/PPy (1:2) layers, increases the operating frequency and the total losses of the system and, in turn, influences negatively on the gas sensing performance of the sensors. This is in line with other systems, in which large amount of catalyst added to the sensitive material have shown to decrease the sensor sensitivity [180]. In this context, hereafter, the gas tests were focussed on the sensors with lower QD loadings (CdTe/PPy (1:10)) as representatives of the CdTe/PPy composite based sensors.

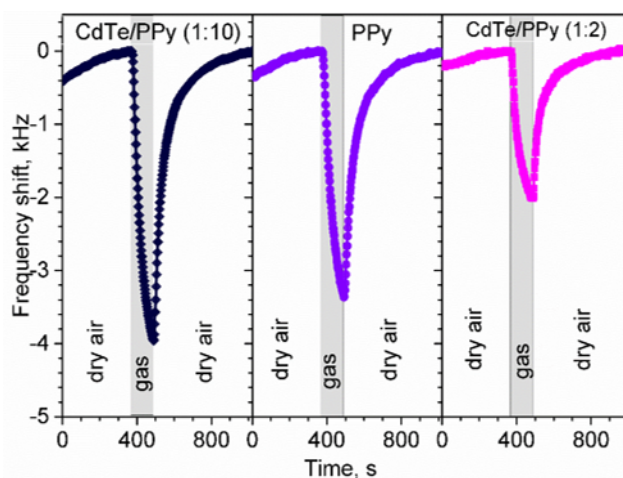


Figure 5.3: Response of CdTe/PPy (1:10) (black line), PPy (purple line) and CdTe/PPy (1:2) (pink line) L-SAW sensors to 5 ppm of acetone.

The sensitivity of the L-SAW sensors was defined as the ratio between the change in sensor response for a fixed change in analyte concentration (between 1 and 5 ppm for this study). The mean sensitivity values to acetone, ethanol, and toluene are 652, 441, and 260 Hz/ppm for the PPy sensors and 771, 546, and 303 Hz/ppm for the CdTe/PPy (1:10) L-SAW sensors. This shows that the sensitivity of the CdTe/PPy (1:10) sensors was improved by a factor of ~ 1.2 compared to the PPy L-SAW sensors for all tested analytes. Moreover, the higher sensitivities to acetone for both the PPy and CdTe/PPy (1:10) sensors were observed, with cross sensitivities (ΔS) to ethanol and toluene of 211 and 392 Hz/ppm for PPy, respectively and 225 and 468 Hz/ppm for CdTe/PPy (1:10), respectively. This indicates a good sensitivity and a partial selectivity in both sensors to acetone.

The results showed that the PPy and CdTe/PPy (1:10) L-SAW sensors respond better to polar (acetone and ethanol) than to non-polar (toluene) gases. This behaviour could be caused by the polar nature of the sensitive layer (i.e., the PPy-PVA blend), which facilitates the dipole-dipole interaction with other polar molecule. Previously, it was also observed that the polar polymers (e.g., polythiophene) also showed an improved sensitivity to polar VOCs, including alcohols and ketones, compared to nonpolar analytes (e.g., aromatic hydrocarbons) [181]. Interestingly, the sensitivity order of the L-SAW sensors to tested analytes is also correlated with the polarity of each analyte. For instance, the sensors show better response to analytes with higher dipole moments (i.e., higher molecular polarity) [182] than to those with lower dipole moments. Thus, the dipole moments of acetone (2.88 D), ethanol (1.69 D) and toluene (0.38 D) correspond with the order of sensitivity registered. In this context, the dipole-dipole interactions of the positively polarized side in pyrrole ($N^{\delta-}-H^{\delta+}$) and/or the hydroxyl group in PVA ($-O^{\delta-}-H^{\delta+}$) with the negatively polarized side of functional groups in acetone ($>C^{\delta-}=O^{\delta-}$) or ethanol ($-O^{\delta-}-H^{\delta+}$) lead to the formation of hydrogen bond (see Figure 5.4 a). This might lead to stronger interactions between PPy and the polar molecules compared to non-polar molecules [183] and, in turn, to better sensor responses to acetone and ethanol than to toluene. The FTIR analysis of the sensors before and after exposure to acetone model analyte (Figure 5.4 b) is also in line with this statement, as we observe a lowering of the O-H stretching band frequency in PPy from 3520 cm^{-1} to 3473 cm^{-1} after acetone exposure [184], which

points out the formation of hydrogen bond between PPy and acetone molecules. The changes in shape, intensity and slightly in position of the bands between 1652 and 1462 cm^{-1} (stretching of C=N, C-N, C-N-H or C=C bonds) and the band at 1711 cm^{-1} (stretching of C=O bond) also suggest interactions between the N-H bond of PPy and the C=O bonds of acetone. This is also consistent with the adsorption of acetone at the PPy surface.

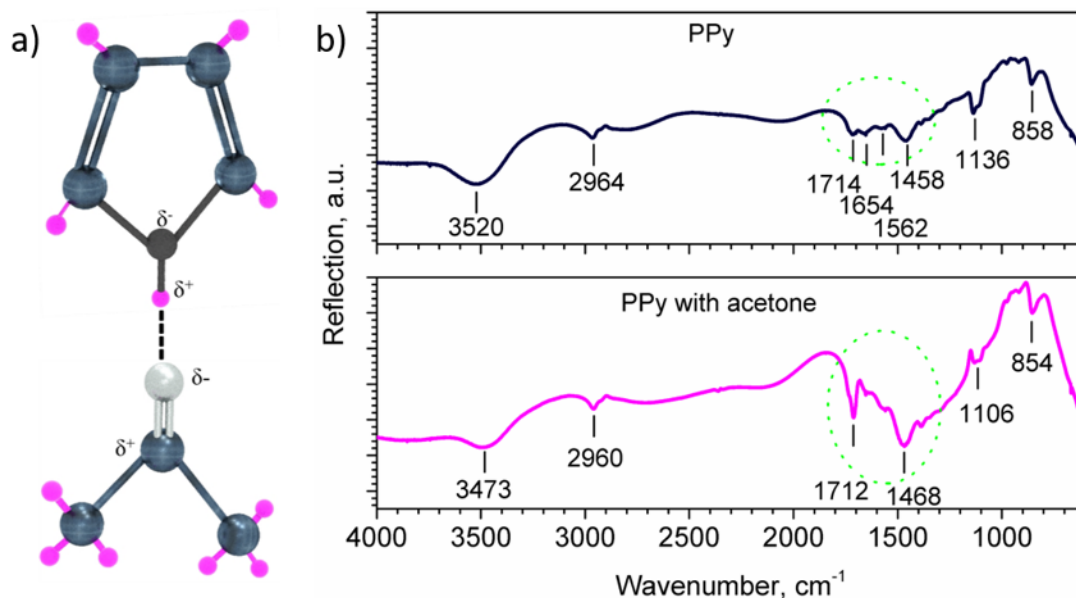


Figure 5.4: Schematic illustration of dipole-dipole interaction (hydrogen bond) between pyrrole and acetone molecules (a). FTIR spectra of PPy L-SAW sensors before (black line) and after (pink line) exposure to acetone (b).

The LOD for the CdTe/PPy (1:10) L-SAW sensors to acetone was estimated to be 5 ppb, while the frequency shifts of this sensors to 5 ppm of acetone change from 4 kHz in dry air to 1.8 and 0.9 kHz at 10 % and 30 % RH, respectively.

In summary, systematic gas sensing tests of the L-SAW sensors showed that the magnitude of responses to these vapors changes from the highest to the lowest in the following order: CdTe/PPy (1:10) > PPy > CdTe/PPy (1:2). Generally, the CdTe/PPy (1:10) L-SAW sensors show better responses to acetone with a sensitivity of 771 Hz/ppm, estimated LOD of 5 ppb and low cross-sensitivities to ethanol and to toluene. The enhanced sensing performance of the CdTe/PPy (1:10) L-SAW sensors to acetone was attributed in part to the catalytic activity of the QDs and the adsorption of acetone at PPy via dipole-dipole interaction. In contrast, the low responses of the CdTe/PPy (1:2) sensors are connected with the agglomeration of QDs on the PPy layer and, thus, a deviation in an operation frequency and insertion loss of these sensors compared to the PPy and CdTe/PPy (1:10) sensors.

5.3 Conclusions

The development of inorganic-organic nanocomposites based on mixture of PPy NPs with CdTe QDs was achieved. The results confirmed the important role of the doping materials and their loadings in the overall sensing properties of L-SAW sensors. Thus, when the host material (PPy) was doped with the relatively low amounts of QDs (CdTe/PPy (1:10)), the decrease in the velocity of the acoustic wave was achieved and therefore, the enhancement in the functional properties of this L-SAW sensor was noticed. However, the use of high amounts of QDs (CdTe/PPy (1:2)) contributed to the formation of larger clusters within the second guiding/sensitive layer, which resulted in the creation of systems with higher operation frequency and insertion loss. Those type of properties influenced negatively the gas sensing performance of the L-SAW sensors.

Chapter 6

Summary of results and conclusions

In this dissertation, the investigation of non-modified and modified PPy nanostructures and their integration into gas sensing devices was presented. The motivation behind this work was to examine the properties of PPy based materials and their sensing performances, in order to develop a cheap gas sensor which enables for the detection of specific gases and VOCs such as ammonia, acetone, ethanol, ethylene and toluene.

The work summarizes the development of five different PPy systems, including two non-modified in the form of NRs and NPs, and three modified based on functionalized PPy NPs with Au NPs, Ag NPs and CdTe QDs. Many complementary analytical techniques (microscopic and spectroscopic) were used for the determination of morphology and chemical composition of synthesized PPy nanostructures. Moreover, Raman and XPS spectroscopic techniques also showed to be an insightful tool for *in-situ* gas sensing test. Raman and XPS *in-situ* gas sensing test revealed the potential of PPy NRs and PPy NPs to sense ammonia and to be used as a gas sensitive material. However, beside the nature of material and chemical predisposition, the efficient integration of sensing material with a particular electronic system (a transducing platform) is the key factor for the accomplishment of the sensing capability (see Table 6.1). Accordingly, the complex design of PPy NRs chemo-resistive sensors and the extremely high resistance (in the range of G Ω) of PPy NPs based chemo-resistive sensors were the main reasons for their incapability. Nevertheless, the 'simple' design of L-SAW sensors based on PPy NPs resulted in the development of the gas sensors with outstanding performances.

Table 6.1: Comparison of gas sensing response of PPy based chemo-resistive and L-SAW sensors to ammonia (NH₃) and ethanol (C₂H₆O). The response of L-SAW sensors is showed as the frequency shift in kHz, while the response of chemo-resistive sensors is presented as R_a/R_g, where R_a and R_g is resistance in air and gas, respectively. The response of L-SAW sensors has negative value, as the frequency was decreased during the gas exposure.

Material	Type of sensor	C (ppm)	Response	
			NH ₃	C ₂ H ₆ O
PPy NRs	Chemo-resistive	100	1	Not tested
PPy NPs	Chemo-resistive	80	Not tested	1
PPy NPs	L-SAW	5	0.4	2.9
Au/PPy (1:10)	Chemo-resistive	80	Not tested	1.6
Au/PPy (1:10)	L-SAW	5	1.4	3.8
Ag/PPy	Chemo-resistive	80	Not tested	1
Ag/PPy	L-SAW	5	Not tested	4.7

In order to create the L-SAW sensors with enhanced performances, various material combinations were investigated in this thesis. Also, the sensitive layers with different thickness were tested by changing the deposition conditions. In total, eight different PPy based multi-guiding L-SAW sensors were fabricated, and their properties and sensing abilities are summarized in Table 6.2. The results showed that the final sensing performances of the L-SAW sensors are dependent on the choice of the second guiding/sensitive

layer, but also the velocity of the propagated wave has a strong influence.

The propagation velocity and attenuation of Love wave are determined by the properties of the second guiding/sensitive layer such as thickness, stiffness, roughness, etc. Normally, as the thickness of the guiding/sensitive layer increases, the operation frequency of sensor should decrease, and the sensors with lower operation frequency (slower wave velocity) and appropriate insertion loss may provide higher mass sensitivity. Our results are in the line with those facts. The higher response and/or sensitivity of the non-modified PPy sensors to acetone, ethanol and toluene is observed for the sensor with the lower operation frequency (161.8 MHz) than by the one with higher frequency (162.5 MHz). This can be ascribed to slower velocity of the Love wave in the thicker PPy layer. The same observations are also noticed in the case of the sensors based on CdTe/PPy. Accordingly, the CdTe/PPy (1:2) sensor with higher operation frequency of 163.8 MHz showed the lower response and/or sensitivity to acetone, ethanol and toluene compared to CdTe/PPy (1:10) which had the operation frequency of 162.4 MHz. In both cases, the second/guiding layer is made of the material with the same chemical structure, thus, the differences in the response and/or sensitivity of two sensors could be caused by the different velocity of the wave in those layers. However, the higher sensitivity of Ag/PPy and Au/PPy sensors to acetone, ethanol and toluene compared to non-modified PPy sensor is caused by the presence of the catalytic nanoparticles rather than by the different operation frequency. Minimal variations of ± 0.3 MHz in the operation frequency are observed among those sensors. In the same line, the CdTe/PPy (1:10) sensors established higher response compared to non-modified PPy sensor. This improvement in response could be assigned to the presence of the hybrid material, as the difference in the operation frequency of those sensors is ± 0.1 MHz.

Table 6.2: Summary and comparison of the L-SAW sensor characteristics and their gas sensing performances to target analytes: acetone (C_3H_6O), ammonia (NH_3), ethanol (C_2H_6O), ethylene (C_2H_4) and toluene (C_7H_8). All developed sensors have multi-guiding layer concept, where the first guiding layer is made of SiO_2 (3 μm thick) and the second guiding layer is corresponding sensitive layer deposited with spin coating velocity of 2500 or 4000 rpm. The response of the sensors is presented for 5 ppm of the target gas. The sensitivity was defined as the ratio between the change in sensor response for a fixed change in analyte concentration (between 2 and 10 ppm for ammonia and ethylene, and between 1 and 5 ppm for acetone, ethanol and toluene). The insertion loss and response have negative value.

SL	V (rpm)	d (nm)	f (MHz)	II (dB)	R (Hz)			S (Hz/ppm)						
PPy	4000	250	161.6	23	NH ₃	C ₂ H ₄	NH ₃	C ₂ H ₄						
					374	360	50	84						
					1380	652	89	152						
Au/PPy (1:10)		350	161.4	22										
Au/PPy (1:2)		400	161.2	22	513	1325	112	271						
PPy	2500	260	161.8	22	C ₃ H ₆ O	C ₂ H ₆ O	C ₇ H ₈	C ₃ H ₆ O	C ₂ H ₆ O	C ₇ H ₈				
					3456	3119	1573	670	551	260				
					4700	4212	2143	876	738	340				
Ag/PPy (1:10)		260	161.5	19										
Au/PPy (1:10)		500	161.7	22	4156	3750	1915	776	656	302				
PPy	4000	250	162.5	22	3374	2879	1554	652	441	250				
					CdTe/PPy (1:10)	250	162.4	22	3967	3566	1859	771	546	308
					CdTe/PPy (1:2)	100	163.8	32	2029	1874	988	379	280	162

SL - second guiding/sensitive layer, V - velocity of spin coater, d - thickness of second guiding/sensitive layer (with errors of ± 10 nm), f - operation frequency of sensor, II - insertion loss of sensors, R - response of sensor, S - sensitivity.

In conclusion, the results achieved in this thesis, demonstrated the fabrication of L-SAW sensors with high mass sensitivity. This was achieved thanks to the choice of sensing material and slow transfer wave velocity presented in the multi-guiding layer concept where elastic layer of SiO_2 is combined with viscos-elastic layer based on PPy nanostructures. The objective of cost effective fabrication of simple micro-sensing elements with ability to sense all selected gases and VOCs was fulfilled. Among the tested sensing layers, modified PPy layer with Ag NPs and/or Au NPs deposited with spin coating velocity of 2500 rpm can be selected as the best technological solution for the fabrication of L-SAW sensors for the detection of acetone in dry and humid (at RH up to 30 %) environment. The improved sensing performances accomplish at RT operation, such as high sensitivity and low LOD, make these sensors a good candidate for the potential use in applications such as breath analysis for diagnostic purposes, as well as quality monitoring of air and food. However, before Ag/PPy and/or Au/PPy L-SAW sensors can be exploit in future consumer devices, the further technological solutions for the detection of acetone in the presence of large amount of moisture (RH > 30 %) remain to be investigated. Thus, the use of dehydration elements in the system or moisture filter with a specific pore channels which ensures that target gas molecules can easily pass through it, while it blocks the water molecules, could be helpful [109].

Bibliography

- [1] BARBRI, N. E. et al. An electronic nose system based on a micro-machined gas sensor array to assess the freshness of sardines. *Sensors and Actuators B: Chemical*, 2009, vol. 141, no. 2, pp. 538-543. ISSN 0925-4005.
- [2] PENG, G. et al. Detection of lung, breast, colorectal, and prostate cancers from exhaled breath using a single array of nanosensors. *British Journal of Cancer*, 2010, vol. 103, no. 4, pp. 542-551. ISSN 0007-0920.
- [3] MORANDI, S. et al. Operational functionalities of air-quality WSn metal-oxide sensors correlating semiconductor defect levels and surface potential barriers. *Science of The Total Environment*, 2020, vol. 706, pp. 135731. ISSN 0048-9697.
- [4] ZENG, Y. M. et al. Two-dimensional nanomaterials for gas sensing applications: the role of theoretical calculations. *Nanomaterials*, 2018, vol. 8, no. 10, pp. 16. ISSN 2079-4991.
- [5] JI, H. C. et al. Gas sensing mechanisms of metal oxide semiconductors: a focus review. *Nanoscale*, 2019, vol. 11, no. 47, pp. 22664-22684. ISSN 2040-3364.
- [6] MIRZAEI, A. et al. Nanostructured semiconducting metal oxide gas sensors for acetaldehyde detection. *Chemosensors*, 2019, vol. 7, no. 4, pp. 16.
- [7] SUN, Y. F. et al. Metal oxide nanostructures and their gas sensing properties: a review. *Sensors*, 2012, vol. 12, no. 3, pp. 2610-2631. ISSN 1424-8220.
- [8] KOO, W.-T. et al. Catalyst-decorated hollow WO₃ nanotubes using layer-by-layer self-assembly on polymeric nanofiber templates and their application in exhaled breath sensor. *Sensors and Actuators B: Chemical*, 2016, vol. 223, pp. 301-310. ISSN 0925-4005.
- [9] WANG, Y. et al. NH₃ gas sensing performance enhanced by Pt-loaded on mesoporous WO₃. *Sensors and Actuators B: Chemical*, 2017, vol. 238, pp. 473-481. ISSN 0925-4005.
- [10] ZHANG, S. et al. Self-assembled hierarchical Au-loaded In₂O₃ hollow microspheres with superior ethanol sensing properties. *Sensors and Actuators B: Chemical*, 2016, vol. 231, pp. 245-255. ISSN 0925-4005.
- [11] LI, M. et al. Ultrasensitive and highly selective detection of methoxy propanol based on Ag-decorated SnO₂ hollow nanospheres. *Sensors and Actuators B: Chemical*, 2016, vol. 232, pp. 545-556. ISSN 0925-4005.
- [12] LEE, S. W. et al. Recent advances in carbon material-based NO₂ gas sensors. *Sensors and Actuators B: Chemical*, 2018, vol. 255, pp. 1788-1804. ISSN 0925-4005.
- [13] LLOBET, E. Gas sensors using carbon nanomaterials: A review. *Sensors and Actuators B: Chemical*, 2013, vol. 179, pp. 32-45. ISSN 0925-4005.
- [14] WANG, Y. M. et al. Sensors based on conductive polymers and their composites: a review. *Polymer International*, 2019, vol. 69, no. 1, pp. 11. ISSN 0959-8103.
- [15] YOON, H. Current trends in sensors based on conducting polymer nanomaterials. *Nanomaterials*, 2013, vol. 3, no. 3, pp. 524-549. ISSN 2079-4991.
- [16] CHOUDHURY, A. Polyaniline/silver nanocomposites: dielectric properties and ethanol vapour sensitivity. *Sensors and Actuators B: Chemical*, 2009, vol. 138, no. 1, pp. 318-325. ISSN 0925-4005.

- [17] KABIR, L. et al. Humidity-sensing properties of conducting polypyrrole-silver nanocomposites. *Journal of Experimental Nanoscience*, 2008, vol. 3, no. 4, pp. 297-305. ISSN 1745-8080.
- [18] LEE, J.-S. et al. Au-polypyrrole framework nanostructures for improved localized surface plasmon resonance volatile organic compounds gas sensing. *Journal of Nanoscience and Nanotechnology*, 2015, vol. 15, no. 10, pp. 7738-7742. ISSN 1533-4880.
- [19] ATHAWALE, A. A. et al. Nanocomposite of Pd-polyaniline as a selective methanol sensor. *Sensors and Actuators B: Chemical*, 2006, vol. 114, no. 1, pp. 263-267. ISSN 0925-4005.
- [20] HUANG, J. et al. Gas sensing performance of polyaniline/ZnO organic-inorganic hybrids for detecting VOCs at low temperature. *Journal of Natural Gas Chemistry*, 2011, vol. 20, no. 5, pp. 515-519. ISSN 1003-9953.
- [21] JOULAZADEH, M. a NAVARCHIAN, A. H. Ammonia detection of one-dimensional nanostructured polypyrrole/metal oxide nanocomposites sensors. *Synthetic Metals*, 2015, vol. 210, pp. 404-411. ISSN 0379-6779.
- [22] BACHHAV, S. G. a PATIL, D. R. Study of polypyrrole-coated MWCNT nanocomposites for ammonia sensing at room temperature. *Journal of Materials Science and Chemical Engineering*, 2015, vol. 3, pp. 30-44.
- [23] DANESHKHAH, A. et al. Poly(vinylidene fluoride-hexafluoropropylene) composite sensors for volatile organic compounds detection in breath. *Sensors and Actuators B: Chemical*, 2015, vol. 221, pp. 635-643. ISSN 0925-4005.
- [24] TUNG, T. T. et al. Graphene-Fe₃O₄/PIL-PEDOT for the design of sensitive and stable quantum chemo-resistive VOC sensors. *Carbon*, 2014, vol. 74, pp. 104-112. ISSN 0008-6223.
- [25] FENG, X. M. et al. The synthesis of shape-controlled polypyrrole/graphene and the study of its capacitance properties. *Polymer Bulletin*, 2013, vol. 70, no. 8, pp. 2291-2304. ISSN 0170-0839.
- [26] GUERNION, N. et al. The fabrication and characterisation of a highly sensitive polypyrrole sensor and its electrical responses to amines of differing basicity at high humidities. *Synthetic Metals*, 2002, vol. 126, no. 2-3, pp. 301-310. ISSN 0379-6779.
- [27] ZHANG, L. et al. A novel ammonia sensor based on high density, small diameter polypyrrole nanowire arrays. *Sensors and Actuators B: Chemical*, 2009, vol. 142, no. 1, pp. 204-209. ISSN 0925-4005.
- [28] ATHAWALE, A. A. a KULKARNI, M. V. Polyaniline and its substituted derivatives as sensor for aliphatic alcohols. *Sensors and Actuators B-Chemical*, 2000, vol. 67, no. 1-2, pp. 173-177. ISSN 0925-4005.
- [29] KIM, J.-S. et al. Fabrication and sensing behavior of PVF₂ coated-polyaniline sensor for volatile organic compounds. *Sensors and Actuators B: Chemical*, 2005, vol. 108, no. 1-2, pp. 409-413. ISSN 0925-4005.
- [30] EAIDKONG, T. et al. Polydiacetylene paper-based colorimetric sensor array for vapor phase detection and identification of volatile organic compounds. *Journal of Materials Chemistry*, 2012, vol. 22, no. 13, pp. 5970-5977. ISSN 0959-9428.
- [31] YOON, J. et al. Colorimetric sensors for volatile organic compounds (VOCs) based on conjugated polymer-embedded electrospun fibers. *Journal of the American Chemical Society*, 2007, vol. 129, no. 11, pp. 3038-3039. ISSN 0002-7863.
- [32] MALKESHI, H. a MILANI MOGHADDAM, H. Ammonia gas-sensing based on polythiophene film prepared through electrophoretic deposition method. *Journal of Polymer Research*, 2016, vol. 23, no. 6, pp. 108. ISSN 1572-8935.
- [33] KIM, T. a KWAK, D. Flexible VOC sensors using conductive polymers and porous membranes for application to textiles. *Fibers and Polymers*, 2012, vol. 13, no. 4, pp. 471-474. ISSN 1229-9197.

- [34] PARK, E. et al. One-pot synthesis of silver nanoparticles decorated poly(3,4-ethylenedioxythiophene) nanotubes for chemical sensor application. *Journal of Materials Chemistry*, 2012, vol. 22, no. 4, pp. 1521-1526. ISSN 0959-9428.
- [35] KAISER, M. R. et al. Electro-polymerized polypyrrole film for fabrication of flexible and slurry-free polypyrrole-sulfur-polypyrrole sandwich electrode for the lithium-sulfur battery. *Journal of Power Sources*, 2019, vol. 437, pp. 226925. ISSN 0378-7753.
- [36] LUO, S. J. et al. Self-standing polypyrrole/black phosphorus laminated film: promising electrode for flexible supercapacitor with enhanced capacitance and cycling stability. *ACS Applied Materials & Interfaces*, 2018, vol. 10, no. 4, pp. 3538-3548. ISSN 1944-8244.
- [37] NOWICKA, A. M. et al. Polypyrrole-au nanoparticles composite as suitable platform for dna biosensor with electrochemical impedance spectroscopy detection. *Electrochimica Acta*, 2014, vol. 140, pp. 65-71. ISSN 0013-4686.
- [38] NAYAK, A. K. et al. Hierarchical nanostructured WO₃-SnO₂ for selective sensing of volatile organic compounds. *Nanoscale*, 2015, vol. 7, no. 29, pp. 12460-12473. ISSN 2040-3364.
- [39] DALAVI, D. S. et al. Nanoporous network of nickel oxide for ammonia gas detection. *Materials Letters*, 2015, vol. 146, pp. 103-107. ISSN 0167-577X.
- [40] LI, Y. S. et al. High-aspect-ratio single-crystalline porous In₂O₃ nanobelts with enhanced gas sensing properties. *Journal of Materials Chemistry*, 2011, vol. 21, no. 34, pp. 12852-12857. ISSN 0959-9428.
- [41] NA, C. W. et al. Transformation of ZnO nanobelts into single-crystalline Mn₃O₄ nanowires. *ACS Applied Materials & Interfaces*, 2012, vol. 4, no. 12, pp. 6565-6572. ISSN 1944-8244.
- [42] PETER MARTIN, L. et al. Effect of Cr₂O₃ electrode morphology on the nitric oxide response of a stabilized zirconia sensor. *Sensors and Actuators B: Chemical*, 2003, vol. 96, no. 1, pp. 53-60. ISSN 0925-4005.
- [43] WANG, S. et al. Organic/inorganic hybrid sensors: A review. *Sensors and Actuators B: Chemical*, 2013, vol. 182, pp. 467-481. ISSN 0925-4005.
- [44] HAKIM, M. et al. Volatile organic compounds of lung cancer and possible biochemical pathways. *Chemical Reviews*, 2012, vol. 112, no. 11, pp. 5949-5966. ISSN 0009-2665.
- [45] HAICK, H. a COHEN-KAMINSKY, S. Detecting lung infections in breathprints: empty promise or next generation diagnosis of infections. *European Respiratory Journal*, 2015, vol. 45, no. 1, pp. 21-24. ISSN 0903-1936.
- [46] VAN DE KANT, K. D. G. et al. Clinical use of exhaled volatile organic compounds in pulmonary diseases: a systematic review. *Respiratory Research*, 2012, vol. 13, pp. 1-23. ISSN 1465-993X.
- [47] PACHECO, J. G. et al. Molecularly imprinted electrochemical sensor for the point-of-care detection of a breast cancer biomarker (CA 15-3). *Sensors and Actuators B-Chemical*, 2018, vol. 256, pp. 905-912. ISSN 0925-4005.
- [48] ZONTA, G. et al. Detection of colorectal cancer biomarkers in the presence of interfering gases. *Sensors and Actuators B-Chemical*, 2015, vol. 218, pp. 289-295. ISSN 0925-4005.
- [49] DI FRANCESCO, F. et al. Breath analysis: trends in techniques and clinical applications. *Microchemical Journal*, 2005, vol. 79, no. 1, pp. 405-410. ISSN 0026-265X.
- [50] RAMÍREZ, N. et al. Chronic risk assessment of exposure to volatile organic compounds in the atmosphere near the largest Mediterranean industrial site. *Environment International*, 2012, vol. 39, no. 1, pp. 200-209. ISSN 0160-4120.
- [51] BAI, J. et al. Aroma profile characterization of Mahi-Mahi and tuna for determining spoilage using purge and trap gas chromatography-mass spectrometry. *Journal of Food Science*, 2019, vol. 84, no. 3, pp. 481-489. ISSN 0022-1147.
- [52] FINK, T. et al. Ion mobility spectrometry in breath research. *Journal of Breath Research*, 2014, vol. 8, no. 2, pp. 1-11. ISSN 1752-7155.

- [53] LIGOR, M. et al. Determination of volatile organic compounds in exhaled breath of patients with lung cancer using solid phase microextraction and gas chromatography mass spectrometry. *Clinical Chemistry and Laboratory Medicine*, 2009, vol. 47, no. 5, pp. 550-560. ISSN 1434-6621.
- [54] AHMED, W. M. et al. Exhaled volatile organic compounds of infection: A systematic review. *ACS Infectious Diseases*, 2017, vol. 3, no. 10, pp. 695-710. ISSN 2373-8227.
- [55] SUN, J. et al. Volatile organic compounds emissions from traditional and clean domestic heating appliances in Guanzhong Plain, China: Emission factors, source profiles, and effects on regional air quality. *Environment International*, 2019, vol. 133, pp. 105252. ISSN 0160-4120.
- [56] KIM, H.-J. a LEE, J.-H. Highly sensitive and selective gas sensors using p-type oxide semiconductors: Overview. *Sensors and Actuators B: Chemical*, 2014, vol. 192, pp. 607-627. ISSN 0925-4005.
- [57] STETTER, J. R. a LI, J. Amperometric gas sensors - A review. *Chemical Reviews*, 2008, vol. 108, no. 2, pp. 352-366. ISSN 0009-2665.
- [58] BAHARUDDIN, A. A. et al. Advances in chemiresistive sensors for acetone gas detection. *Materials Science in Semiconductor Processing*, 2019, vol. 103, pp. 104616. ISSN 1369-8001.
- [59] CALHEIRO, D. S. a BIANCHI, R. F. Tuning the detection limit in hybrid organic-inorganic materials for improving electrical performance of sensing devices. *Sensors and Actuators A: Physical*, 2019, vol. 298, pp. 111480. ISSN 0924-4247.
- [60] DONG, C. et al. A review on WO₃ based gas sensors: morphology control and enhanced sensing properties. *Journal of Alloys and Compounds*, 2020, vol. 820, pp. 153194. ISSN 0925-8388.
- [61] FENG, S. B. et al. Review on smart gas sensing technology. *Sensors*, 2019, vol. 19, no. 17, pp. 22.
- [62] GARDON, M. a GUILMANY, J. M. A review on fabrication, sensing mechanisms and performance of metal oxide gas sensors. *Journal of Materials Science: Materials in Electronics*, 2013, vol. 24, no. 5, pp. 1410-1421. ISSN 1573-482X.
- [63] AFZAL, A. et al. Advanced vapor recognition materials for selective and fast responsive surface acoustic wave sensors: a review. *Analytica Chimica Acta*, 2013, vol. 787, pp. 36-49. ISSN 0003-2670.
- [64] YAACOB, M. H. et al. Optical response of WO₃ nanostructured thin films sputtered on different transparent substrates towards hydrogen of low concentration. *Sensors and Actuators B: Chemical*, 2013, vol. 177, pp. 981-988. ISSN 0925-4005.
- [65] ARAFAT, M. M. et al. Gas sensors based on one dimensional nanostructured metal-oxides: a review. *Sensors*, 2012, vol. 12, no. 6, pp. 7207-7258. ISSN 1424-8220.
- [66] RIGHETTONI, M. et al. Breath analysis by nanostructured metal oxides as chemo-resistive gas sensors. *Materials Today*, 2015, vol. 18, no. 3, pp. 163-171. ISSN 1369-7021.
- [67] TOMIC, M. et al. Cerium oxide-tungsten oxide core-shell nanowire-based microsensors sensitive to acetone. *Biosensors-Basel*, 2018, vol. 8, no. 4, pp. 11.
- [68] MILLER, D. R. et al. Nanoscale metal oxide-based heterojunctions for gas sensing: a review. *Sensors and Actuators B: Chemical*, 2014, vol. 204, pp. 250-272. ISSN 0925-4005.
- [69] SKOTHEIM, T. A. a REYNOLDS, J. Conjugated polymers: theory, synthesis, properties, and characterization. CRC Press, 2006, ISBN 9781420043594.
- [70] CELIESIUTE, R. et al. Electrochromic sensors based on conducting polymers, metal oxides, and coordination complexes. *Critical Reviews in Analytical Chemistry*, 2019, vol. 49, no. 3, pp. 195-208. ISSN 1040-8347.
- [71] LONG, Y.-Z. et al. Recent advances in synthesis, physical properties and applications of conducting polymer nanotubes and nanofibers. *Progress in Polymer Science*, 2011, vol. 36, no. 10, pp. 1415-1442. ISSN 0079-6700.
- [72] WANG, Y. Q. et al. Conductive polymers for stretchable supercapacitors. *Nano Research*, 2019, vol. 12, no. 9, pp. 1978-1987. ISSN 1998-0124.

- [73] LE, T. H. et al. Electrical and electrochemical properties of conducting polymers. *Polymers*, 2017, vol. 9, no. 4, pp. 32. ISSN 2073-4360.
- [74] MA, Z. et al. Doping engineering of conductive polymer hydrogels and their application in advanced sensor technologies. *Chemical Science*, 2019, vol. 10, no. 25, pp. 6232-6244. ISSN 2041-6520.
- [75] BREDAS, J. L. a STREET, G. B. Polarons, bipolarons, and solitons in conducting polymers. *Accounts of Chemical Research*, 1985, vol. 18, no. 10, pp. 309-315. ISSN 0001-4842.
- [76] PARK, S. J. et al. Conducting polymer-based nanohybrid transducers: A potential route to high sensitivity and selectivity sensors. *Sensors*, 2014, vol. 14, no. 2, pp. 3604-3630. ISSN 1424-8220.
- [77] ZHANG, L. et al. Recent progress on nanostructured conducting polymers and composites: synthesis, application and future aspects. *Science China-Materials*, 2018, vol. 61, no. 3, pp. 303-352. ISSN 2095-8226.
- [78] JACKOWSKA, K. et al. Hard template synthesis of conducting polymers: a route to achieve nanostructures. *Journal of Solid State Electrochemistry*, 2008, vol. 12, no. 4, pp. 437-443. ISSN 1432-8488.
- [79] SHAH, K. W. et al. One-dimensional nanostructure engineering of conducting polymers for thermoelectric applications. *Applied Sciences-Basel*, 2019, vol. 9, no. 7, pp. 22.
- [80] JACKOWSKA, K. et al. Hard template synthesis of conducting polymers: a route to achieve nanostructures. *Journal of Solid State Electrochemistry*, 2008, vol. 12, no. 4, pp. 437-443. ISSN 1433-0768.
- [81] GHOSH, S. et al. Nanostructured conducting polymers for energy applications: towards a sustainable platform. *Nanoscale*, 2016, vol. 8, no. 13, pp. 6921-6947. ISSN 2040-3364.
- [82] ZHANG, X. et al. Controllable synthesis of conducting polypyrrole nanostructures. *The Journal of Physical Chemistry B*, 2006, vol. 110, no. 3, pp. 1158-1165. ISSN 1520-6106.
- [83] DIAZ-ORELLANA, K. P. a ROBERTS, M. E. Scalable, template-free synthesis of conducting polymer microtubes. *Rsc Advances*, 2015, vol. 5, no. 32, pp. 25504-25512. ISSN 2046-2069.
- [84] WONG, Y. C. et al. Review-conducting polymers as chemiresistive gas sensing materials: a review. *Journal of the Electrochemical Society*, 2019, vol. 167, no. 1. ISSN 0013-4651.
- [85] GENG, L. a WU, S. Preparation, characterization and gas sensitivity of polypyrrole/ γ -Fe₂O₃ hybrid materials. *Materials Research Bulletin*, 2013, vol. 48, no. 10, pp. 4339-4343. ISSN 0025-5408.
- [86] HAMILTON, S. et al. Polypyrrole materials for detection and discrimination of volatile organic compounds. *Sensors and Actuators B: Chemical*, 2005, vol. 107, no. 1, pp. 424-432. ISSN 0925-4005.
- [87] BENIWAL, A. a SUNNY Electrospun SnO₂/PPy nanocomposite for ultra-low ammonia concentration detection at room temperature. *Sensors and Actuators B: Chemical*, 2019, vol. 296, pp. 126660. ISSN 0925-4005.
- [88] LI, S. et al. Room temperature gas sensor based on tin dioxide@ polyaniline nanocomposite assembled on flexible substrate: ppb-level detection of NH₃. *Sensors and Actuators B: Chemical*, 2019, vol. 299, pp. 126970. ISSN 0925-4005.
- [89] YU, X. et al. Digital ammonia gas sensor based on quartz resonator tuned by interdigital electrode coated with polyaniline film. *Organic Electronics*, 2020, vol. 76, pp. 105413. ISSN 1566-1199.
- [90] CHEN, X. et al. Gas sensing properties of surface acoustic wave NH₃ gas sensor based on Pt doped polypyrrole sensitive film. *Sensors and Actuators B: Chemical*, 2013, vol. 177, pp. 364-369. ISSN 0925-4005.
- [91] USMAN, F. et al. Enhanced sensitivity of surface plasmon resonance biosensor functionalized with doped polyaniline composites for the detection of low-concentration acetone vapour. *Journal of Sensors*, 2019, vol. 2019, pp. 13. ISSN 1687-725X.

- [92] BAGCHI, S. et al. Electrospun polypyrrole-polyethylene oxide coated optical fiber sensor probe for detection of volatile compounds. *Sensors and Actuators B-Chemical*, 2017, vol. 250, pp. 52-60.
- [93] LAKARD, B. et al. Gas sensors based on electrodeposited polymers. *Metals*, 2015, vol. 5, no. 3, pp. 1371-1386. ISSN 2075-4701.
- [94] PARK, S. J. et al. Chemo-electrical gas sensors based on conducting polymer hybrids. *Polymers*, 2017, vol. 9, no. 5, pp. 24.
- [95] SANJUÁN, A. M. et al. Recent developments in sensing devices based on polymeric systems. *Reactive and Functional Polymers*, 2018, vol. 133, pp. 103-125. ISSN 1381-5148.
- [96] BAI, H. a SHI, G. Q. Gas sensors based on conducting polymers. *Sensors*, 2007, vol. 7, no. 3, pp. 267-307. ISSN 1424-8220.
- [97] CHOUGULE, M. A. et al. Polypyrrole thin film: room temperature ammonia gas sensor. *IEEE Sensors Journal*, 2011, vol. 11, no. 9, pp. 2137-2141. ISSN 2379-9153.
- [98] YADAV, A. A. et al. Synthesis and characterization of polypyrrole thin film by MW-CBD method for NH₃ gas sensor. *Polymer Bulletin*, 2018, vol. 75, no. 10, pp. 4547-4553. ISSN 1436-2449.
- [99] TANG, X. et al. An ammonia sensor composed of polypyrrole synthesized on reduced graphene oxide by electropolymerization. *Sensors and Actuators B: Chemical*, 2020, vol. 305, pp. 127423. ISSN 0925-4005.
- [100] SHARMA, A. L. et al. Nanostructured polyaniline films on silicon for sensitive sensing of ammonia. *Sensors and Actuators A: Physical*, 2013, vol. 198, pp. 107-112. ISSN 0924-4247.
- [101] SUTAR, D. S. et al. Preparation of nanofibrous polyaniline films and their application as ammonia gas sensor. *Sensors and Actuators B: Chemical*, 2007, vol. 128, no. 1, pp. 286-292. ISSN 0925-4005.
- [102] WANG, H. et al. 3D Hollow quasi-graphite capsules/polyaniline hybrid with a high performance for room-temperature ammonia gas sensors. *ACS Sensors*, 2019, vol. 4, no. 9, pp. 2343-2350. ISSN 2379-3694.
- [103] NAVALE, S. T. et al. Room temperature NO₂ sensing properties of polythiophene films. *Synthetic Metals*, 2014, vol. 195, pp. 228-233. ISSN 0379-6779.
- [104] BAI, S. L. et al. Enhancement of NO₂-sensing performance at room temperature by graphene-modified polythiophene. *Industrial & Engineering Chemistry Research*, 2016, vol. 55, no. 19, pp. 5788-5794. ISSN 0888-5885.
- [105] SEEKAEW, Y. et al. Low-cost and flexible printed graphene-PEDOT:PSS gas sensor for ammonia detection. *Organic Electronics*, 2014, vol. 15, no. 11, pp. 2971-2981. ISSN 1566-1199.
- [106] ŠETKA, M. et al. Nanostructured polypyrrole-based ammonia and volatile organic compound sensors. *Sensors*, 2017, vol. 17, no. 3, pp. 28.
- [107] KWON, O. S. et al. Novel flexible chemical gas sensor based on poly(3,4-ethylenedioxythiophene) nanotube membrane. *Talanta*, 2010, vol. 82, no. 4, pp. 1338-1343. ISSN 0039-9140.
- [108] LI, S. Y. et al. Flexible ammonia sensor based on PEDOT:PSS/silver nanowire composite film for meat freshness monitoring. *Ieee Electron Device Letters*, 2017, vol. 38, no. 7, pp. 975-978. ISSN 0741-3106.
- [109] LIU, W. et al. A highly sensitive and moisture-resistant gas sensor for diabetes diagnosis with Pt@In₂O₃ nanowires and a molecular sieve for protection. *Npg Asia Materials*, 2018, vol. 10, pp. 293-308. ISSN 1884-4049.
- [110] KWON, O. S. et al. Resistive gas sensors based on precisely size-controlled polypyrrole nanoparticles: effects of particle size and deposition method. *Journal of Physical Chemistry C*, 2010, vol. 114, no. 44, pp. 18874-18879. ISSN 1932-7447.
- [111] KWON, O. S. et al. Highly sensitive and selective chemiresistive sensors based on multidimensional polypyrrole nanotubes. *Chemical Communications*, 2012, vol. 48, no. 85, pp. 10526-10528. ISSN 1359-7345.

- [112] XUE, M. Q. et al. High-oriented polypyrrole nanotubes for next-generation gas sensor. *Advanced Materials*, 2016, vol. 28, no. 37, pp. 8265-8270. ISSN 0935-9648.
- [113] YAN, Y. R. et al. Viral-templated gold/polypyrrole nanopeapods for an ammonia gas sensor. *Nanotechnology*, 2016, vol. 27, no. 32, pp. 9. ISSN 0957-4484.
- [114] CHARTUPRAYOON, N. et al. Wafer-scale fabrication of single polypyrrole nanoribbon-based ammonia sensor. *Journal of Physical Chemistry C*, 2010, vol. 114, no. 25, pp. 11103-11108. ISSN 1932-7447.
- [115] JOULAZADEH, M. a NAVARCHIAN, A. H. Alcohol sensibility of one-dimensional polyaniline and polypyrrole nanostructures. *Ieee Sensors Journal*, 2015, vol. 15, no. 3, pp. 1697-1704. ISSN 1530-437X.
- [116] LEE, J.-S. et al. Au-polypyrrole framework nanostructures for improved localized surface plasmon resonance volatile organic compounds gas sensing. *Journal of Nanoscience and Nanotechnology*, 2015, vol. 15, no. 10, pp. 7738-7742. ISSN 1533-4880.
- [117] QIN, H. Y. et al. Polypyrrole thin film fiber optic chemical sensor for detection of VOCs. *Sensors and Actuators B-Chemical*, 2011, vol. 158, no. 1, pp. 223-228. ISSN 0925-4005.
- [118] CAMPOS, M. et al. Influence of methane in the electrical properties of polypyrrole films doped with dodecylbenzene sulfonic acid. *Sensors and Actuators B-Chemical*, 2007, vol. 125, no. 1, pp. 158-166. ISSN 0925-4005.
- [119] CAMPOS, M. a IEEE. Gas sensing properties based on a doped conducting polymer/inorganic semiconductor. In *Proceedings of the Ieee Sensors 2003, Vols 1 and 2. 2003*, pp. 1126-1129.
- [120] XU, Y. W. et al. Detection and identification of breast cancer volatile organic compounds biomarkers using highly-sensitive single nanowire array on a chip. *Journal of Biomedical Nanotechnology*, 2013, vol. 9, no. 7, pp. 1164-1172. ISSN 1550-7033.
- [121] BHATT, C. M. a JAMPANA, N. Multi frequency interrogation of polypyrrole based gas sensors for organic vapors. *Microsystem Technologies-Micro-and Nanosystems-Information Storage and Processing Systems*, 2011, vol. 17, no. 3, pp. 417-423. ISSN 0946-7076.
- [122] MUSIO, F. a FERRARA, M. C. Low frequency a.c. response of polypyrrole gas sensors. *Sensors and Actuators B-Chemical*, 1997, vol. 41, no. 1-3, pp. 97-103. ISSN 0925-4005.
- [123] LIU, X. et al. A survey on gas sensing technology. *Sensors*, 2012, vol. 12, no. 7, pp. 9635-9665. ISSN 1424-8220.
- [124] HANGARTER, C. M. et al. Hybridized conducting polymer chemiresistive nano-sensors. *Nano Today*, 2013, vol. 8, no. 1, pp. 39-55. ISSN 1748-0132.
- [125] CAPONE, S. et al. Solid state gas sensors: State of the art and future activities. *Journal of Optoelectronics and Advanced Materials*, 2003, vol. 5, no. 5, pp. 1335-1348. ISSN 1454-4164.
- [126] EGGINS, B. R. *Chemical sensors and biosensors*. Wiley, 2008, ISBN 9780470511312.
- [127] MOSELEY, P. T. Progress in the development of semiconducting metal oxide gas sensors: a review. *Measurement Science and Technology*, 2017, vol. 28, no. 8, pp. 15. ISSN 0957-0233.
- [128] FANGET, S. et al. Gas sensors based on gravimetric detection—A review. *Sensors and Actuators B: Chemical*, 2011, vol. 160, no. 1, pp. 804-821. ISSN 0925-4005.
- [129] YANASE, Y. et al. Diagnosis of immediate-type allergy using surface plasmon resonance. *Optical Materials Express*, 2016, vol. 6, no. 4, pp. 1339-1348. ISSN 2159-3930.
- [130] WOHLTJEN, H. Mechanism of operation and design considerations for surface acoustic wave device vapour sensors. *Sensors and Actuators*, 1984, vol. 5, no. 4, pp. 307-325. ISSN 0250-6874.
- [131] IPPOLITO, S. J. et al. Acoustic wave gas and vapor sensors, *Solid State Gas Sensing*. Boston, MA: Springer US, 2009, pp. 1-44.

- [132] BRYANT, A. et al. Gas detection using surface acoustic wave delay lines. *Sensors and Actuators*, 1983, vol. 4, no. Supplement C, pp. 105-111. ISSN 0250-6874.
- [133] MATATAGUI, D. et al. Array of Love-wave sensors based on quartz/Novolac to detect CWA simulants. *Talanta*, 2011, vol. 85, no. 3, pp. 1442-1447. ISSN 0039-9140.
- [134] DUFLOS, G. et al. Determination of volatile compounds to characterize fish spoilage using headspace/mass spectrometry and solid-phase microextraction/gas chromatography/mass spectrometry. *Journal of the Science of Food and Agriculture*, 2006, vol. 86, no. 4, pp. 600-611. ISSN 0022-5142.
- [135] LI, W. W. et al. A cross-sectional study of breath acetone based on diabetic metabolic disorders. *Journal of Breath Research*, 2015, vol. 9, no. 1, pp. 9. ISSN 1752-7155.
- [136] WANG, C. et al. A Study on breath acetone in diabetic patients using a cavity ringdown breath analyzer: exploring correlations of breath acetone with blood glucose and glycohemoglobin A1C. *IEEE Sensors Journal*, 2010, vol. 10, no. 1, pp. 54-63. ISSN 2379-9153.
- [137] ULANOWSKA, A. et al. The application of statistical methods using VOCs to identify patients with lung cancer. *Journal of Breath Research*, 2011, vol. 5, no. 4, pp. 11. ISSN 1752-7155.
- [138] RUZSANYI, V. a KALAIPOS, M. P. Breath acetone as a potential marker in clinical practice. *Journal of Breath Research*, 2017, vol. 11, no. 2, pp. 18. ISSN 1752-7155.
- [139] SPANEL, P. et al. Breath acetone concentration; biological variability and the influence of diet. *Physiological Measurement*, 2011, vol. 32, no. 8, pp. N23-N31. ISSN 0967-3334.
- [140] HUANG, Y. et al. Evaluation and characterization of volatile air toxics indoors in a heavy polluted city of northwestern China in wintertime. *Science of The Total Environment*, 2019, vol. 662, pp. 470-480. ISSN 0048-9697.
- [141] GOODMAN, N. B. et al. Indoor volatile organic compounds at an Australian university. *Building and Environment*, 2018, vol. 135, pp. 344-351. ISSN 0360-1323.
- [142] MITRAN, E. et al. Neurotoxicity associated with occupational exposure to acetone, methyl ethyl ketone, and cyclohexanone. *Environmental Research*, 1997, vol. 73, no. 1-2, pp. 181-188. ISSN 0013-9351.
- [143] EZHILAN, M. et al. An Electronic nose for royal delicious apple quality assessment – a tri-layer approach. *Food Research International*, 2018, vol. 109, pp. 44-51. ISSN 0963-9969.
- [144] DELAHOZ, R. E. et al. Chronic lung disease secondary to ammonia inhalation injury: A report on three cases. *American Journal of Industrial Medicine*, 1996, vol. 29, no. 2, pp. 209-214. ISSN 0271-3586.
- [145] TIMMER, B. et al. Ammonia sensors and their applications—a review. *Sensors and Actuators B: Chemical*, 2005, vol. 107, no. 2, pp. 666-677. ISSN 0925-4005.
- [146] LEDUC, D. et al. Acute and long-term respiratory damage following inhalation of ammonia. *Thorax*, 1992, vol. 47, no. 9, pp. 755-757. ISSN 0040-6376.
- [147] POPA, C. et al. Ethylene and ammonia traces measurements from the patients' breath with renal failure via LPAS method. *Applied Physics B-Lasers and Optics*, 2011, vol. 105, no. 3, pp. 669-674. ISSN 0946-2171.
- [148] OBERMEIER, J. et al. Exhaled volatile substances mirror clinical conditions in pediatric chronic kidney disease. *Plos One*, 2017, vol. 12, no. 6, pp. 18. ISSN 1932-6203.
- [149] IACUMIN, L. et al. A new cause of spoilage in goose sausages. *Food Microbiology*, 2016, vol. 58, pp. 56-62. ISSN 0740-0020.
- [150] ZHANG, B. et al. Identification of beef spoilage via the analysis of volatiles using long optical-path Fourier transform infrared spectroscopy. *Analytical Methods*, 2015, vol. 7, no. 14, pp. 5891-5897. ISSN 1759-9660.

- [151] CABALLERO, A. a SEGURA, A. The quest for lower alcoholic wines. *Microbial Biotechnology*, 2017, vol. 10, no. 2, pp. 238-241. ISSN 1751-7915.
- [152] CONTRERAS, M. D. M. et al. Usefulness of GC-IMS for rapid quantitative analysis without sample treatment: Focus on ethanol, one of the potential classification markers of olive oils. *LWT*, 2020, vol. 120, pp. 108897. ISSN 0023-6438.
- [153] MITSUBAYASHI, K. et al. Bioelectronic sniffers for ethanol and acetaldehyde in breath air after drinking. *Biosensors and Bioelectronics*, 2005, vol. 20, no. 8, pp. 1573-1579. ISSN 0956-5663.
- [154] GOLDNER, M. C. et al. Effect of ethanol level in the perception of aroma attributes and the detection of volatile compounds in red wine. *Journal of Sensory Studies*, 2009, vol. 24, no. 2, pp. 243-257. ISSN 0887-8250.
- [155] GUOHUA, H. et al. Study of peach freshness predictive method based on electronic nose. *Food Control*, 2012, vol. 28, no. 1, pp. 25-32. ISSN 0956-7135.
- [156] TURNER, C. et al. A longitudinal study of ethanol and acetaldehyde in the exhaled breath of healthy volunteers using selected-ion flow-tube mass spectrometry. *Rapid Communications in Mass Spectrometry*, 2006, vol. 20, no. 1, pp. 61-68. ISSN 0951-4198.
- [157] GOERL, T. et al. Volatile breath biomarkers for patient monitoring during haemodialysis. *Journal of Breath Research*, 2013, vol. 7, no. 1, pp. 8. ISSN 1752-7155.
- [158] MATTOO, A. K. *The Plant Hormone Ethylene*. CRC Press, 2018. pp. ISBN 9781351092661.
- [159] CAPRIOLI, F. a QUERCIA, L. Ethylene detection methods in post-harvest technology: A review. *Sensors and Actuators B: Chemical*, 2014, vol. 203, pp. 187-196. ISSN 0925-4005.
- [160] HU, B. et al. Recent advances in detecting and regulating ethylene concentrations for shelf-life extension and maturity control of fruit: A review. *Trends in Food Science & Technology*, 2019, vol. 91, pp. 66-82. ISSN 0924-2244.
- [161] SARAIVA, L. A. et al. Thap Maeo bananas: Fast ripening and full ethylene perception at low doses. *Food Research International*, 2018, vol. 105, pp. 384-392. ISSN 0963-9969.
- [162] LI, Y. et al. Continuous exposure to ethylene in the storage environment adversely affects 'Afourer' mandarin fruit quality. *Food Chemistry*, 2018, vol. 242, pp. 585-590. ISSN 0308-8146.
- [163] PAARDEKOOOPER, L. M. et al. Ethylene, an early marker of systemic inflammation in humans. *Scientific Reports*, 2017, vol. 7, pp. 10. ISSN 2045-2322.
- [164] PETRUS, M. et al. Spectroscopic analysis of breath ethylene and oxidative stress relation with glycaemic status in type 2 diabetes. *Optical and Quantum Electronics*, 2016, vol. 49, no. 1, pp. 2. ISSN 1572-817X.
- [165] CRISTESCU, S. M. et al. Real-time monitoring of endogenous lipid peroxidation by exhaled ethylene in patients undergoing cardiac surgery. *American Journal of Physiology-Lung Cellular and Molecular Physiology*, 2014, vol. 307, no. 7, pp. 509-515. ISSN 1040-0605.
- [166] POPA, C. et al. The level of ethylene biomarker in the renal failure of elderly patients analyzed by photoacoustic spectroscopy. *Laser Physics*, 2013, vol. 23, no. 12, pp. 4. ISSN 1054-660X.
- [167] FENG, R. et al. Ethylene, xylene, toluene and hexane are major contributors of atmospheric ozone in Hangzhou, China, prior to the 2022 Asian Games. *Environmental Chemistry Letters*, 2019, vol. 17, no. 2, pp. 1151-1160. ISSN 1610-3653.
- [168] KELLER, N. et al. Ethylene removal and fresh product storage: a challenge at the frontiers of chemistry. toward an approach by photocatalytic oxidation. *Chemical Reviews*, 2013, vol. 113, no. 7, pp. 5029-5070. ISSN 0009-2665.
- [169] GREENBERG, M. M. The central nervous system and exposure to toluene: A risk characterization. *Environmental Research*, 1997, vol. 72, no. 1, pp. 1-7. ISSN 0013-9351.

- [170] LOCK, E. A. et al. Solvents and Parkinson disease: A systematic review of toxicological and epidemiological evidence. *Toxicology and Applied Pharmacology*, 2013, vol. 266, no. 3, pp. 345-355. ISSN 0041-008X.
- [171] FILLEY, C. M. et al. The effects of toluene on the central nervous system. *Journal of Neuropathology and Experimental Neurology*, 2004, vol. 63, no. 1, pp. 1-12. ISSN 0022-3069.
- [172] ALONSO, M. et al. Evaluation of potential breath biomarkers for active smoking: assessment of smoking habits. *Analytical and Bioanalytical Chemistry*, 2010, vol. 396, no. 8, pp. 2987-2995. ISSN 1618-2642.
- [173] LIGOR, T. et al. The analysis of healthy volunteers' exhaled breath by the use of solid-phase microextraction and GC-MS. *Journal of Breath Research*, 2008, vol. 2, no. 4, pp. 8. ISSN 1752-7155.
- [174] SETKA, M. et al. Raman and XPS studies of ammonia sensitive polypyrrole nanorods and nanoparticles. *Scientific Reports*, 2019, vol. 9, pp. 10. ISSN 2045-2322.
- [175] ŠETKA, M. et al. Gold/polypyrrole nanorods for gas sensing application. *Proceedings of SPIE - The International Society for Optical Engineering. Barcelona, Spain: Smart Sensors, Actuators, and MEMS VIII*, 2018, vol. 10246.
- [176] ŠETKA, M. et al. Love wave sensors based on gold nanoparticle-modified polypyrrole and their properties to ammonia and ethylene. *Sensors and Actuators B: Chemical*, 2019, vol. 304, pp. 127337. ISSN 0925-4005.
- [177] ŠETKA, M. et al. Love wave sensors with silver modified polypyrrole nanoparticles for VOCs monitoring. *Sensors*, 2020, vol. 20, no. 5, pp. 1432. ISSN 1424-8220.
- [178] SIMEUNOVIĆ, J. P. et al. Studying of quantum dot luminescence quenching effect caused by covalent conjugation with protein. *Monatshefte für Chemie - Chemical Monthly*, 2017, vol. 148, no. 11, pp. 1901-1909. ISSN 1434-4475.
- [179] FRAGOSO-MORA, J. R. et al. Gas sensors based on elasticity changes of nanoparticle layers. *Sensors and Actuators B: Chemical*, 2018, vol. 268, pp. 93-99. ISSN 0925-4005.
- [180] CHO, H.-J. et al. Pt-functionalized pdo nanowires for room temperature hydrogen gas sensors. *ACS Sensors*, 2018, vol. 3, no. 10, pp. 2152-2158.
- [181] LI, B. et al. Volatile organic compound detection using nanostructured copolymers. *Nano Letters*, 2006, vol. 6, no. 8, pp. 1598-1602. ISSN 1530-6984.
- [182] GENG, W. C. et al. Volatile organic compound gas-sensing properties of bimodal porous alpha-Fe₂O₃ with ultrahigh sensitivity and fast response. *ACS Applied Materials & Interfaces*, 2018, vol. 10, no. 16, pp. 13702-13711. ISSN 1944-8244.
- [183] HAMILTON, S. et al. Polypyrrole materials for detection and discrimination of volatile organic compounds. *Sensors and Actuators B: Chemical*, 2005, vol. 107, no. 1, pp. 424-432. ISSN 0925-4005.
- [184] LIN-VIEN, D. et al. *The handbook of infrared and raman characteristic frequencies of organic molecules*. Elsevier Science, 1991. ISBN 9780080571164.